A multi-hierarchical approach reveals D-serine as a hidden substrate of sodium-coupled monocarboxylate transporters

Pattama Wiriyasermkul[1,2,3,a], Satomi Moriyama[3], Masataka Suzuki[4], Pornparn Kongpracha[1,2], Nodoka Nakamae[3], Saki Takeshita[3], Yoko Tanaka[3], Akina Matsuda[4], Masaki Miyasaka[1,2], Kenji Hamase[5], Tomonori Kimura[6,7], Masashi Mita[8], Jumpei Sasabe[4], Shushi Nagamori[1,2,3*]

[1]Center for SI Medical Research, [2]Department of Laboratory Medicine, The Jikei University School of Medicine, Tokyo, Japan

[3]Department of Collaborative Research for Biomolecular Dynamics, Nara Medical University, Nara, Japan

[4]Department of Pharmacology, Keio University School of Medicine, Tokyo, Japan

[5]Graduate School of Pharmaceutical Sciences, Kyushu University, Fukuoka, Japan

[6]KAGAMI Project, [7]Reverse Translational Research Project, Center for Rare Disease Research, National Institutes of Biomedical Innovation, Health and Nutrition (NIBIOHN). Osaka, Japan

[8]KAGAMI Inc., Osaka, Japan

* Corresponding author: Shushi Nagamori

Email: snagamori@nagamori-lab.jp

[a] Present address: Department of Biological Chemistry and Food Science, Faculty of Agriculture, Iwate University, Iwate, Japan

Keywords

transporter, amino acid, kidney diseases, micronutrient, biomarker

Abstract

Transporter research primarily relies on the canonical substrates of well-established transporters. This approach has limitations when studying transporters for the low-abundant micromolecules, such as micronutrients, and may not reveal physiological functions of the transporters. While D-serine, a trace enantiomer of serine in the circulation, was discovered as an emerging biomarker of kidney function, its transport mechanisms in the periphery remain unknown. Here, using a multi-hierarchical approach from body fluids to molecules, combining multi-omics, cell-free synthetic biochemistry, and *ex vivo* transport analyses, we have identified two types of renal D-serine transport systems. We revealed that the small amino acid transporter ASCT2 serves as a D-serine transporter previously uncharacterized in the kidney and discovered D-serine as a noncanonical substrate of the sodium-coupled monocarboxylate transporters (SMCTs). These two systems are physiologically complementary, but ASCT2 dominates the role in the pathological condition. Our findings not only shed light on renal D-serine transport, but also clarify the importance of non-canonical substrate transport. This study provides a framework for investigating multiple transport systems of various trace micromolecules under physiological conditions and in multifactorial diseases.

Introduction

Membrane transport proteins function to transport micromolecules such as nutrients, ions, and metabolites across membranes, thereby playing a pivotal role in the regulation of micromolecular homeostasis. To date, over 450 solute carriers (SLCs), 40 ATP-binding cassettes (ABCs), 60 ATPase pumps, and 300 ion channels have been identified in mammals (Ranjan et al., 2011; César-Razquin et al., 2015; Perland and Fredriksson, 2017; The UniProt Consortium et al., 2021). Approximately 30% of membrane transport proteins remain uncharacterized. While some membrane transport proteins can be classified based on sequence similarities and transport substrates of well-studied family members, this approach is limited when it comes to discovering transporters for some micromolecules, such as micronutrients and their metabolites. Many of these micromolecules have not been extensively studied and do not fit into traditional nutrient types. Currently, the importance of micronutrients and gut microbiota-derived metabolites in health and disease has gained a high impact (Shenkin, 2006; Vernocchi et al., 2016; Liu et al., 2022), yet their responsible transporters are not well understood. Understanding the absorption and reabsorption mechanisms of dietary micronutrients and gut microbiota-derived metabolites will provide a key molecular process for controlling their dynamics and molecular activities.

This study aims to establish an approach to investigate the physiological function and pathological significance of transporters, particularly transport systems for trace micromolecules. As a paradigm, we investigated renal transport systems for D-amino acids, micronutrients derived mostly from the diet and some from the gut microbiota. Amino acid transport systems have been well studied (Bröer, 2008a), but have focused on L-amino acids, which are macronutrients, leaving open the question of how D-amino acids are transported. We have developed two-dimensional high-performance liquid chromatography (2D-HPLC), which allows the segregation of L- and D-enantiomers in liquid biopsy (Miyoshi et al., 2009; Hamase

et al., 2010). The importance of D-amino acids in renal function has received increasing attention (Sasabe et al., 2014; Kimura et al., 2016; Sasabe and Suzuki, 2018; Nakade et al., 2018; Hesaka et al., 2019; Kimura et al., 2020; Okushima et al., 2021; Iwata et al., 2022; Suzuki et al., 2022). D-Serine in the body fluid was discovered as a promising biomarker for acute kidney injury (AKI) and chronic kidney disease (CKD) due to its clear association with kidney function in rodents and humans (Sasabe et al., 2014; Kimura et al., 2016; Nakade et al., 2018; Hesaka et al., 2019; Okushima et al., 2021). Diseased-associated alterations in plasma and urinary D-/L-serine ratio suggest that renal D-serine transport systems are different and distinct from L-serine transport systems under physiological and pathological conditions. The transport of D-serine has long been found to take place at the proximal tubules (Kragh-Hansen and Sheikh, 1984; Shimomura et al., 1988; Silbernagl et al., 1999; Sasabe and Suzuki, 2018), yet the corresponding transporter has not been clearly elucidated.

D-Serine is found at submillimolar levels in the brain (Hashimoto et al., 1992), where it acts as an obligatory physiological co-agonist of *N*-methyl-D-aspartate receptors (NMDARs) (Mothet et al., 2000; Basu et al., 2009; Papouin et al., 2012; Wolosker, 2018). Extensive studies of D-serine in the brain show that D-serine is transported by four plasma membrane transporters: ASCT1 (SLC1A4), ASCT2 (SLC1A5), Asc-1 (SLC7A10), and SNAT1 (SLC38A1) (Rosenberg et al., 2013; Foster et al., 2016; Kaplan et al., 2018; Bodner et al., 2020). In contrast, D-serine is detected at low micromolar levels in the periphery, and little is known about its dynamics as well as transport systems. Mammals acquire D-serine by biosynthesis via serine racemase function (Wolosker et al., 1999) and absorption from the diet and gut microbiota presumably via intestinal transport system(s) (Sasabe and Suzuki, 2018; Nakade et al., 2018; Gonda et al., 2023). Similar to the renal epithelia, a D-serine transporter in the intestine is also unknown.

89 In this study, we integrated multiple analytical methods for the different biological
90 hierarchies. We applied 2D-HPLC to quantify the plasma and urinary enantiomers of 20 amino
91 acids of renal ischemia-reperfusion injury (IRI) mice, a model of AKI and AKI-to-CKD
92 transition (Sasabe et al., 2014; Fu et al., 2018). Membrane proteomics of the renal proximal
93 tubules of the IRI mouse models was performed to explore the key molecules responsible for
94 the alterations of D- and L-amino acid transport. With bioinformatics, cell-based screening, and
95 cell-free transport analysis, we identified two types of D-serine transport systems in the kidney.
96 Subsequently, *ex vivo* transport analyses from the normal kidney and the IRI model explained
97 the transport mechanism of D-serine as a biomarker in kidney diseases.

98 # Results

99 **Amino acid metabolomics in plasma and urine of the renal IRI model**

100 To understand kidney-associated alteration of enantiomeric amino acids, we measured
101 L- and D-isomers of 20 amino acids in the body fluids of the IRI model (Figure supplements 1-
102 2). Dynamics of L- and D- enantiomers in the plasma were evaluated from the ratios of D-/L-
103 enantiomers (Figure 1A). Among amino acids, only the ratios of plasma D-/L-serine were
104 increased in a time dependent-manner from 4 – 40 hours after the ischemia-reperfusion (Figure
105 1A-B). The elevation of plasma D-/L-serine ratios at early time points (4h – 8h) was due to a
106 sharp decrease of the L-isomer, while the rise of D-/L-serine ratios at late time points (20h –
107 40h) was a result of a continuous acceleration of the D-isomer (Figure 1C-D). The results of
108 plasma D-serine were consistent with previous observations (Sasabe et al., 2014). In addition
109 to D-serine, we detected certain amounts of D-alanine, D-proline and D-methionine in the
110 plasma (Figure supplement 1A). However, their D-/L- enantiomeric ratios were uncorrelated to
111 the pathological conditions (Figure 1A). Our knowledge of traditional amino acid transport
112 suggests that alanine, serine, and proline share the same transport systems (Bröer, 2008a). The
113 noticeably different profile of plasma D- and L-serine from those of alanine and proline led to
114 the speculation that D-serine transport was possibly mediated by unique transport systems,
115 different from those of D-alanine, D-proline, and the L-isomers. Notably, such transport systems
116 may be sensitive to the IRI conditions.

117 We measured the enantiomeric amino acid profiles from urine samples of the IRI model
118 (Figure supplement 2). While plasma is a reliable resource of metabolite biomarkers, urine is
119 a meaningful non-invasive diagnostic indicator of kidney function. More importantly, the
120 analysis of urinary metabolites is indispensable for elucidating the unknown reabsorption
121 systems of certain substances in the kidney. From our results, the ratios of urinary D-/L-serine

122 were drastically decreased at early IRI (4h – 8h) (Figure 1E-F). Similar tendencies of D-/L-
123 amino acid ratios were observed in alanine, proline, asparagine, and histidine (Figure 1E-H).
124 These urinary amino acid profiles indicated the impairment in both D- and L-amino acid
125 reabsorption since the early injury. We hypothesized that transporters play a major role in the
126 dynamics of D- and L-serine in the kidney with respect to changes in the D-/L-serine ratio during
127 pathology.

128 **Proteomics for membrane transport proteins from renal brush border membranes of the**
129 **IRI model**

130 We aimed to identify the corresponding molecules for the dynamics of D- and L-serine.
131 To obtain the candidates, we performed proteomic analysis of renal brush border membrane
132 vesicles (BBMVs; the membrane fraction enriching apical membrane proteins of proximal
133 tubular epithelia) from the IRI model. We analyzed the BBMVs from 4 – 8 hours after IRI, the
134 times of rigorous shift of plasma and urinary D-/L-serine ratio (Figure 1B, F). The proteomes
135 of the IRI samples were calculated as ratios of the negative control group (sham), yielding two
136 groups of comparative proteome data: 4h IRI/sham (4h) and 8h IRI/sham (8h). In total, 4,423
137 proteins were identified, of which 1,187 proteins (27% of the total detected proteins) were
138 categorized as plasma membrane proteins and extracellular matrix proteins (Table supplement
139 1). We observed a significant increase of two well-known early AKI biomarkers: Ccn1 (Cyr61:
140 Cellular communication network factor 1; 4h IRI/sham = 41.4 folds; 8h IRI/sham = 29.9 folds)
141 and Ngal (Lcn2: Neutrophil gelatinase-associated lipocalin; 4h IRI/sham = 1.8 folds; 8h
142 IRI/sham = 9.5 folds). This finding confirmed the reliability of our proteomics for molecular
143 analysis of early AKI (Table supplement 1) (Marx et al., 2018).

144 From the proteome, we detected 398 membrane transport proteins (325 transporters and
145 73 ion channels). Analysis of all membrane transport proteins by Ingenuity Pathway Analysis

146 (IPA) revealed alterations of the biological function in *Molecular Transport*, which are
147 categorized by the types of their canonical substrates (Table supplement 2). Transport of "all
148 micromolecules" was shown to be drastically decreased from 4h IRI (Figure 2A: Top). This
149 decrease was due to the dramatic reduction of transport systems for heavy metals and organic
150 compounds (Figure 2A). Figure 2B shows membrane transport proteins corresponding to the
151 annotation in Figure 2A. This proteomic result unveiled the whole picture of the molecular
152 targets of the injury. Furthermore, the results revealed the key membrane transport proteins
153 behind AKI metabolite biomarkers. It is noted that some transporters were upregulated,
154 suggesting the compensatory-mechanism repair processes for cell survival from the injury
155 (Figure 2B).

156 **ASCT2 is one of D-serine transporters at the apical membrane of renal proximal tubules**

157 Given insight into transporters in the proteome, we observed the elevation of mouse
158 Slc1a5/Asct2, a known D-serine transporter in the brain, at both 4h and 8h IRI (Figure 2B:
159 Transport of Amino acids). Asct2 was previously detected in renal brush border membranes,
160 but its precise localization and function in the kidney have not been characterized (Avissar et
161 al., 2001; Scalise et al., 2018). We then examined the localization of Asct2 in the kidney by
162 using affinity-purified Asct2 antibodies that recognized its N-terminus (NT) or C-terminus
163 (CT) (Figure supplement 3A). Asct2 was partially co-immunostained with both Sglt2 (Slc5a2;
164 sodium/glucose cotransporter 2) and Agt1 (Slc7a13, aspartate/glutamate transporter 1), which
165 are apical membrane markers for S1 + S2 and S3 segments, respectively (Figure 3A-B)
166 (Nagamori et al., 2016a; Ghezzi et al., 2018). In contrast, Asct2 did not co-localize with
167 Na^+/K^+-ATPase, a basolateral membrane marker (Figure 3C). The results demonstrated that
168 Asct2 is localized at the apical side in all segments of proximal tubules.

169 To confirm the D-serine transport function of ASCT2 in human cells, we used wild-
170 type (WT) near-haploid human leukemic cancer cell line (HAP1) and HAP1 cells carrying
171 CRISPR/CAS-mediated *ASCT2* knockout (ASCT2-KO). D-serine uptake was significantly
172 decreased in the ASCT2-KO cells (Figure 3D). The function of ASCT2 was also verified in
173 human embryonic kidney HEK293 cells, which endogenously express ASCT2, by using
174 ASCT2-knockdown (Figure 3E).

175 **Screening of candidate molecules for D-serine transporters**

176 While we have shown that ASCT2 is a D-serine transporter at the apical membranes of
177 all proximal tubular segments, ASCT2 transports D-serine with high affinity (K_m of 167 μM in
178 oocyte system) but with weak stereoselectivity (Foster et al., 2016). These properties of ASCT2
179 differ from those of the reported D-serine transport systems in the kidney. First, D-serine
180 transport systems in S1 + S2 segments are reported to be different from those in the S3 segment
181 and the kinetics of both systems are in mM range (Kragh-Hansen and Sheikh, 1984; Silbernagl
182 et al., 1999). Silbernagl et al. also suggested that ASCT2 is not (or not only) a D-serine
183 transporter at S3 segment (Silbernagl et al., 1999). Second, the plasma and urinary D-/L-serine
184 profiles from CKD and AKI samples indicated the stereoselectivity of the transporter (Figure
185 1) (Sasabe and Suzuki, 2018). Third, ASCT2 recognizes serine, alanine, and proline, but our
186 enantiomeric amino acid profile in plasma samples showed a distinct D-/L- ratio pattern of
187 serine from alanine and proline (Figure 1B). All data suggest the existence of (an)other D-serine
188 transporter(s).

189 To search for the D-serine transporters, we chose the ratios of mouse Asct2 as the cutoff
190 values of our membrane proteomic data at both 4h and 8h IRI (Figure 4A). Membrane transport
191 proteins showing more alteration than Asct2 at both increased and decreased values were
192 selected because some transporters are known to switch roles upon pathology. Further, we

193 focused on the luminal transporters and omitted transporters that are reported to be located at
194 basolateral membranes and organelles as the BBMVs are enriched apical membrane fractions.
195 Membrane transport proteins that recognize only inorganic ions were also excluded. Finally,
196 ten candidates were selected (Table 1). Slc36a1/Pat1 and Slc6a18/B^0at3, the known small
197 amino acid transporters, were included in the list, although their expressions only passed the
198 cutoff at only one-time point (either 4h or 8h IRI). Slc5a12/Smct2 was also included because
199 Smct1, another member of sodium-coupled monocarboxylate transporter (SMCT) family, was
200 selected as a candidate. Smct2 has a comparable role with Smct1, but both transporters are
201 localized at different segments of the proximal tubules.

202 To analyze the function of the candidate transporters, we selected HEK293 cell line for
203 the screening method because of its high transfection efficiency. Similar to other several
204 common cell lines, HEK293 cells express ASCT2 endogenously. However, we also examined
205 other possible D-serine transport systems in HEK293 cells, aiming to reduce the transport
206 background. Proteomic analysis of the membrane fractions from HEK293 cells identified
207 amino acid transporters as shown in Table supplement 3. Transport activity of D-serine in
208 HEK293 cells showed Na^+ dependency and ASCT2-substrate mediated inhibition (L-Ser, L-
209 Thr, and L-Met) (Figure supplement 3B-C). Ben-Cys (*S*-benzyl-L-cysteine) and GPNA (L-γ-
210 glutamyl-*p*-nitroanilide) inhibited D-serine transport in HEK293 cells similar to that of ASCT2-
211 expressing cells (Bröer et al., 2016), but SLC38 inhibitor MeAIB (2-(methylamino)isobutyric
212 acid) had no effect (Figure supplement 3C). These results indicated that ASCT2 is the main D-
213 serine transporter in HEK293 cells.

214 Due to the absence of any ASCT2-specific inhibitor and the compensatory transport
215 mechanism that occurred in the ASCT2-deletion condition (Bröer et al., 2016), we avoided
216 using the traditional cell-based transport assay for screening. Instead, we established a new
217 screening method based on cell growth. Apart from the studies on D-serine biomarkers in

218 kidney diseases, a previous study found that high concentrations (10 – 20 mM) of D-serine
219 impaired the growth of a human proximal tubular cell line (Okada et al., 2017). We then tested
220 whether high concentrations of D-serine affect HEK293 cell growth. Unlike L-serine which had
221 no effect, D-serine reduced cell growth in a concentration-dependent manner with IC_{50} of 17.4
222 ± 1.05 mM (Figure supplement 3D). In the ASCT2-knockdown cells, the growth inhibition by
223 D-serine was attenuated (Figure 4B), indicating that D-serine suppressing cell growth was
224 caused by ASCT2-mediated D-serine transport.

225 Based on this finding, we utilized cell growth determination assay as the screening
226 method even in the presence of endogenous ASCT2 expression. HEK293 cells were transfected
227 with human candidate genes without ASCT2 knockdown. The transfected cells were treated
228 with either 15 mM (near IC_{50} concentration) or 25 mM (high concentration) D-serine for 2 days,
229 and cell growth was determined. The positive control Asc-1 transfected cells showed a
230 reduction in cell growth, confirming the effectiveness of this assay (Figure 4C-D). Among ten
231 candidates, PAT1 (SLC36A1) and B^0AT3 (SLC6A18) showed higher cell growth than the
232 mock cells, suggesting that PAT1 and B^0AT3 may reduce D-serine influx mediated by
233 endogenous ASCT2. In contrast, SMCT1 (SLC5A8) and SMCT2 (SLC5A12) extended the
234 growth suppression after treatment with both 15 and 25 mM D-serine (Figure 4C-D and Figure
235 supplement 4A-B). Thus, with the hypothesis that the candidate molecule influxes D-serine and
236 brings about growth reduction, we selected both SMCT1 and SMCT2 for further analysis.

237 **Characterization of D-serine transport in SMCTs**

238 SMCTs are known to transport monocarboxylates such as lactate, propionate, and
239 nicotinate in a Na^+-dependent manner (Ganapathy et al., 2008). To characterize D-serine
240 transport in both SMCT1 and SMCT2, we generated Flp-In T-REx 293 cells stably expressing
241 human SMCT1 (FlpInTR-SMCT1) and SMCT2 (FlpInTR-SMCT2). Expression of SMCTs in

242 FlpInTR-SMCT1 and FlpInTR-SMCT2 was verified by Western blot using anti-FLAG
243 antibody to detect FLAG-tagged SMCTs (Figure supplement 5A). SMCT1 and SMCT2
244 expressions remained unchanged upon ASCT2 knockdown (Figure supplement 5A). The
245 function of SMCTs was confirmed by their canonical substrate [^{14}C]nicotinate transport in the
246 SMCT1- and SMCT2-stable cells (Figure supplement 5B-C).

247 The transport functions of SMCTs are inhibited by non-steroidal anti-inflammatory
248 drugs (NSAIDs; e.g., ibuprofen and acetylsalicylate) (Itagaki et al., 2006; Gopal et al., 2007).
249 To verify the contribution of SMCTs to D-serine-reduced cell growth, we added ibuprofen to
250 the growth assay. In contrast to mock, in which ibuprofen has no effect, the growth suppression
251 by D-serine treatment was gradually attenuated by ibuprofen in both FlpInTR-SMCT1 and
252 FlpInTR-SMCT2 cells, indicating that the cell growth suppression by D-serine treatment is the
253 result of SMCT1 and SMCT2 functions (Figure 5A).

254 We characterized SMCTs mediating D-[^{3}H]serine transport by using SMCT-stable cell
255 lines. Both FlpInTR-SMCT1 and FlpInTR-SMCT2 cells transported D-[^{3}H]serine over Mock
256 (Figure 5B). In the cells with ASCT2 knockdown, the background level was lower, thereby
257 enhancing the D-[^{3}H]serine transport contributed by both SMCT1 and SMCT2 (the net uptake
258 after subtracted with background) (Figure 5C). The D-[^{3}H]serine transport was inhibited by
259 ibuprofen and acetylsalicylate, confirming the specific transport by SMCTs (Figure 5D). The
260 excess of non-radioisotope-labeled D-serine also inhibited D-[^{3}H]serine uptake in both SMCTs.
261 Still, its inhibitory effect in SMCT2 was much less than in SMCT1, suggesting the lower
262 affinity of D-serine in SMCT2 than in SMCT1 (Figure 5D).

263 **D-Serine transport properties and kinetics in SMCT1**

264 Kinetics of D-[^{3}H]serine transport in SMCT1 was measured in FlpInTR-SMCT1 cells
265 in the presence of ASCT2 knockdown. SMCT1 transported D-[^{3}H]serine in a concentration-

266 dependent manner and the curve fitted to Michaelis−Menten kinetics with the apparent K_m of
267 3.39 ± 0.79 mM and V_{max} of 18.23 ± 1.73 pmol/μg protein/min (Figure 5E and Figure
268 supplement 5D).

269 The substrate selectivity of SMCT1 was investigated using synthetic biochemistry to
270 avoid the interference of amino acid and carboxylate transports by endogenous transporters in
271 cells. We established a cell-free assay system using proteoliposomes, in which purified proteins
272 are reconstituted into liposomes and all substances in the system are controllable. We purified
273 human SMCT1 by affinity column and reconstituted SMCT1-proteoliposome (SMCT1-PL)
274 (Figure 6A). The function of SMCT1 in SMCT1-PL was verified by the transport of lactate,
275 propionate, and nicotinate but not urate (negative control) (Figure supplement 6A). The
276 kinetics of [^{14}C]nicotinate transport in SMCT1-PL revealed an apparent K_m of 442 ± 94 μM
277 (Figure supplement 6B), which is in a similar range to the K_m previously described by
278 electrophysiological experiments in *Xenopus* oocyte expression systems (K_m 390 μM) (Paroder
279 et al., 2006), confirming the functional properties of SMCT1 in our cell-free transport assay
280 system.

281 The transport of D-[^{3}H]serine in SMCT1-PL was Na^+-dependent and reached the
282 stationary phase at approximately 5 min (Figure 6B). The amount of D-serine transport was
283 slightly lower than lactate and propionate but higher than L-serine and the transport was
284 inhibited by ibuprofen, confirming SMCT1-mediated D-serine transport (Figure 6C). Amino
285 acid selectivity revealed that SMCT1 recognized both L- and D-serine over other small amino
286 acids (L- and D-alanine), acidic amino acids (L- and D-glutamate), and large neutral amino acids
287 (L- and D-tyrosine) (Figure 6D). Therefore, we concluded that serine is the substrate of SMCT1
288 and the recognition is more stereoselective for the D- than the L-isomer.

289 **ASCT2 and SMCTs contribute to D-serine transport in renal proximal tubular epithelia**

290 We next examined the contributions of ASCT2 and SMCTs to D-serine reabsorption in
291 the kidney using an *ex vivo* transport assay. ASCT2 is an antiporter, influx one amino acid with
292 efflux of another, while SMCTs are symporters (Ganapathy et al., 2008; Scalise et al., 2018).
293 Therefore, we measured D-serine transport in the presence or absence of L-Gln preloading and
294 with or without ibuprofen to distinguish the functions of mouse Asct2 and Smcts. The
295 enantiomeric amino acid profile showed D-serine concentrations of 4 – 10 μM in the plasma
296 samples (Figure supplement 1) and 20 – 100 μM in the urine samples (Figure supplement 2).
297 Accordingly, we tested 10 μM D-[^{3}H]serine transport in BBMVs derived from normal mice. In
298 the non-preloading condition, D-[^{3}H]serine uptake in Na^+ dependence gradually but
299 continuously increased and the uptake was remarkably inhibited by ibuprofen, suggesting that
300 the transport was mainly attained from Smcts functions (Figure 7A). In L-Gln preloaded
301 BBMVs, D-[^{3}H]serine uptake in Na^+-dependence arose quickly and reached the saturated point
302 at 1 – 2 min (Figure 7B). The uptake at early time points (≤ 30 sec) was ibuprofen-insensitive
303 but became partly ibuprofen-sensitive from 1 min to the stationary phase (Figure 7B). These
304 results indicate that the D-serine transport was mediated by both Asct2 and Smcts. At early
305 time points, D-[^{3}H]serine was transported by Asct2, which occurred highly and rapidly.
306 Meanwhile, Smcts functions (ibuprofen-sensitive) initiated later but had prolonged functions
307 as seen in the non-preloading condition. Taken altogether, we suggested that, in the normal
308 kidney where renal proximal tubular epithelial cells contain intracellular L-Gln, D-serine
309 reabsorption is derived from combinational functions of both ibuprofen-sensitive (e.g. Smcts)
310 and ibuprofen-insensitive (e.g. Asct2) transporters.

311 The localization of Smct1 in the kidney was unclear. Gopal et al. reported the
312 localization of Smct1 at S3 and Smct2 in all segments, while single-nucleus RNA sequencing
313 (snRNA-Seq) showed Smct1 at S2 – S3 segments and Smct2 at S1 segment (Figure supplement
314 7: Controls) (Gopal et al., 2007; Kirita et al., 2020). We generated an anti-Smct1 antibody and

315 examined the localization of Smct1. The result showed that Smct1 was mainly localized at the
316 S3 and slightly at the S1 + S2 segments (Figure supplement 8).

317 **D-Serine transport in renal proximal tubular epithelia of IRI model**

318 Under IRI conditions, we observed low urinary but high plasma levels of D-serine,
319 suggesting high D-serine reabsorption (Figure supplements 1A, 2A). Our membrane
320 proteomics revealed that Asct2 was increased while Smct1 and Smct2 were decreased in both
321 4h and 8h IRI (Table 1). We then examined the functional contributions of Asct2 and Smcts
322 on the D-serine reabsorption during the pathology. Similar to those of the normal BBMVs
323 (Figure 7A-B), D-[^{3}H]serine transport in Sham operation showed ibuprofen-sensitive in non-
324 preloading and partly ibuprofen-sensitive in L-Gln preloading conditions (Figure 7C: Sham).
325 D-[^{3}H]Serine influx reduced sharply in the BBMVs of 4h IRI model, and the transport was
326 ibuprofen-insensitive in both with and without L-Gln preloading (Figure 7C: 4h IRI). Likely,
327 this feature was due to the slight increase of Asct2 and the dramatic decrease of Smcts as
328 observed in the proteome data (Asct2: 4h IRI/sham = 1.29 fold, Smct1: 4h IRI/sham = 0.59
329 fold; Smct2: 4h IRI/sham = 0.86 fold; Table supplement 1). We verified that BBMVs from all
330 conditions contain functional proteins by measuring L-[^{3}H]aspartate transport, which
331 represented the function of Slc1a1/Eaac1 (Kanai and Hediger, 1992; Bailey et al., 2011). The
332 assay confirmed that BBMVs derived from 4h IRI model were not fully damaged, although the
333 low influx was likely from the loss of protein expression during the injury (Figure 2B: Amino
334 acids, Figure supplement 9). In the BBMVs of 8h IRI model, D-[^{3}H]serine transport was
335 exceedingly high in L-Gln preloading and it was ibuprofen-insensitive (Figure 7C: L-Gln
336 preloaded). These results could be explained by the continuing increase of Asct2 and decrease
337 of Smcts as revealed by our proteomics (Asct2: 8h IRI/sham = 1.64 fold; Smct1: 8h IRI/sham
338 = 0.62 fold; Smct2: 8h IRI/sham = 0.78 fold) (Table 1, Table supplement 1). The slight increase

339 in D-[^{3}H]serine transport in non-preloaded 8h IRI BBMVs may be due to an unknown
340 transporter (Figure 7C: No preload). Our amino acid profiling showed that the amount of
341 plasma and urinary L-Gln was not largely altered during 4h – 8h IRI (Figures 1B, 2B),
342 suggesting that renal epithelial cells maintain intracellular L-Gln. Most likely, the high
343 reabsorption of D-serine during IRI resulted from the increase of Asct2, despite the decreases
344 of Smct1 and Smct2.

345 For comparison with our proteome data, we analyzed the mRNA expressions of Asct2,
346 Smct1, and Smct2 in proximal tubule clusters at the early IRI from the open-source snRNA-
347 seq dataset (Kirita et al., 2020). Consistent with our proteome data, Smct1 and Smct2 mRNA
348 expressions were dramatically decreased, whereas Asct2 was increased since the early IRI
349 (Figure supplement 7). The correlation of proteomics and transcriptomics suggested that the
350 protein alterations of Asct2 and Smcts during the pathology emerged from transcriptional
351 mechanisms rather than post-translational protein processing or protein degradation. When
352 evaluating the extent of gene/protein alterations between the control and IRI conditions, we
353 observed that the gene alterations of both Asct2 and Smcts, as revealed by snRNA-sequencing,
354 are more pronounced than the protein alteration ratios obtained from proteomics. This
355 discrepancy may stem from difficulty in the quantification method, especially for membrane
356 transport proteins in label-free quantitative proteomics.

357 ## Discussion

358 In this study, we presented an approach to investigate the transport systems for
359 micronutrients and metabolites under physiological conditions and in multifactorial diseases.
360 We selected AKI as a model study because AKI is known to target renal proximal epithelia
361 and disrupt absorption/reabsorption systems that are the results of cooperative functions of
362 multiple transporters. We utilized amino acid metabolomics to reveal a unique feature of the
363 enantiomeric dynamics of serine in the AKI and analyzed membrane proteomes to obtain the
364 D-serine transporter candidates. We then applied cell-based and cell-free transport assays to
365 identify two D-serine transport systems; one was ASCT2 and the other consisted of
366 unanticipated SMCTs (SMCT1 and SMCT2). Using *ex vivo* analysis of apical membrane-
367 enriched renal proximal tubules, we showed that both transport systems contributed
368 comparably to D-serine handling in the normal kidney, but ASCT2 became dominant in AKI,
369 leading to the increase of D-serine in the blood. The alteration of two transport systems
370 explained the dynamics of D-serine and suggested the transport mechanism behind the D-serine
371 biomarker.

372 Several studies have reported the non-canonical substrates of membrane transport
373 proteins, such as the recognition between amino acids, carboxylates and amines among SLCs
374 (Metzner et al., 2005; Matsuo et al., 2008; Schweikhard and Ziegler, 2012; Wei et al., 2016).
375 Serine consists of a hydroxypropionic acid and an amino group at the α-carbon. Possibly, the
376 hydroxypropionic acid on serine is the main part to interact with SMCTs because
377 hydroxypropionic acid shares similar moieties to lactic acid and propionic acid which are the
378 high-affinity substrates of SMCTs. The apparent K_m of D-serine transport in SMCT1 is 3.39
379 mM (Figure 5E), which is within the range of known SMCT1 substrates (0.07 – 6.5 mM)
380 (Ganapathy et al., 2008), suggesting that SMCT1 accepts D-serine in the same manner as other
381 monocarboxylate substrates. Inhibition of D-[^{3}H]serine transport by non-radioisotope labeled

382 D-serine in SMCT2 was less effective than in SMCT1 (Figure 5D). Together with the previous
383 report that SMCT2 had lower inhibition affinities for nicotinate, lactate and butyrate than
384 SMCT1 (Srinivas et al., 2005), we suggest that SMCT2 recognizes D-serine with lower affinity
385 than SMCT1.

386 Kinetics analysis of D-serine transport revealed the high affinity by ASCT2 (K_m 167
387 μM) (Foster et al., 2016) and low affinity by SMCT1 (K_m 3.39 mM; Figure 5E). In addition
388 to transport affinity, the expression levels and co-localization of multiple transporters within
389 the same cells are critical for elucidating the physiological roles of transporters or transport
390 systems (Sakaguchi et al., 2024). In our proteome data, the chromatogram intensities of Smct1
391 (2.9 x 10^9 AU) and Smct2 (1.6 x 10^8 AU) were significantly higher than that of Asct2 (1.5 x
392 10^7 AU) in the control mice (Table 1: abundance in Sham). While direct intensity comparisons
393 between different proteins in mass spectrometry analyses are not precise, they can provide a
394 general indication of relative protein amounts. This finding aligns with the snRNA-seq data,
395 where Asct2 expression was found to be minimal, present in less than 10% of cell populations
396 under both control and IRI conditions, suggesting that many cells do not express Asct2.
397 Conversely, Smct1 and Smct2 show high and ubiquitous expression in control conditions, but
398 their levels are markedly reduced in IRI conditions (Figure supplement 7). Our *ex vivo* assays
399 demonstrate that both ASCT2 and SMCTs mediate D-serine transport (Figure 7B).
400 Consequently, Asct2 may contribute to D-serine reabsorption due to its high affinity, whereas
401 Smcts, owing to their abundance, particularly in cells lacking Asct2, likely play a significant
402 role in D-serine reabsorption. Moreover, factors such as transport turnover rate (K_{cat}) and the
403 presence of local canonical substrates are also vital in defining the overall contribution of D-
404 serine transport systems.

405 Several pieces of evidence support SMCT1 at S3 segment and SMCT2 at S1 + S2
406 segments on renal D-serine handling. First, our enantiomeric amino acid profile from the IRI

407 model, which agrees with the previous reports in CKD patients and AKI animal models,
408 suggested the existence of a stereoselective transport system for serine (Figure 1) (Sasabe et
409 al., 2014; Kimura et al., 2016; Sasabe and Suzuki, 2018; Hesaka et al., 2019; Kimura et al.,
410 2020). The system seems distinct from the known classical small amino acid transport systems
411 and ASCT2. Second, previous studies indicated renal D-serine transport takes place at the
412 proximal tubules by the distinct transport systems between S1 + S2 and S3 segments. Both
413 systems exhibited the characteristics of Na^+ dependency, electrogenicity, low affinity (mM
414 range), and partial stereoselectivity (Kragh-Hansen and Sheikh, 1984; Shimomura et al., 1988;
415 Silbernagl et al., 1999). These properties of the D-serine transport suit well to SMCTs and
416 convince us of the contribution of SMCTs to renal D-serine transport in addition to ASCT2.
417 Moreover, continuous administration of high doses of D-serine induces nephrotoxicity at the
418 S3 segment of proximal tubules in normal animals (Morehead et al., 1945; Silbernagl et al.,
419 1999; Hasegawa et al., 2019). It is most likely that the D-serine-induced proximal tubular
420 damage is partly due to the absorption of D-serine by SMCTs, in particular by SMCT1 at the
421 S3 segment. It is noted that SMCT2 is reported as a protein indicator for kidney repair during
422 the injury. Prolonged SMCT2 down-expression indicates the failed repair of proximal tubular
423 cells in IRI (Kirita et al., 2020). The significance of SMCT2, in turn, supports the merit of D-
424 serine usage in AKI and CKD diagnosis.

425 Combining all the results, we propose the model of D-serine transport systems in renal
426 proximal tubules (Figure 8). In normal kidneys, the expression levels of SMCT2 at S1 + S2
427 segments and SMCT1 at S3 segment are high, whereas ASCT2 is low. Both SMCTs and
428 ASCT2 are involved in D-serine reabsorption. Nonetheless, the net reabsorption levels appear
429 to be relatively low due to the low affinities of SMCTs. It is likely that reabsorption at the S3
430 segment is dominated by SMCT1 function. The reabsorbed D-serine in proximal tubular cells
431 is degraded into OH-pyruvate by D-amino acid oxidase (DAAO), thereby maintaining the low

432 plasma D-serine but high urinary D-serine (Figure 8: Normal). In pathological conditions such
433 as AKI and CKD, the expression levels of SMCT1 and SMCT2 decrease dramatically while
434 ASCT2 increases. The high affinity and ubiquitous expression of ASCT2 suggest the increased
435 D-serine reabsorption in all proximal tubular segments. Together with the in-part reduction of
436 DAAO activity during the pathology (Sasabe et al., 2014), the excess reabsorbed D-serine may
437 lead to a high plasma D-serine level (Figure 8: IRI).

438 The enantiomeric profiles of serine revealed distinct plasma D/L-serine ratios, with low
439 ratios in the normal control but elevated ratios in IRI, despite the weak stereoselectivity of
440 ASCT2 (Figure 1B). This observation suggested the differential renal handling of D-serine
441 compared to L-serine. While we identified SMCTs as a D-serine transport system, it has been
442 reported that L-serine reabsorption is mediated by B^0AT3 (Singer et al., 2009). We propose
443 that the alterations in plasma and urinary D/L-serine ratios are the combined outcomes of: 1)
444 transport systems for L-serine, and 2) transport systems for D-serine. In normal kidneys, the
445 low plasma D/L-serine ratios could result from the efficient reabsorption of L-serine by B^0AT3,
446 coupled with the DAAO activity that degrades intracellular D-serine reabsorbed by SMCTs. In
447 IRI conditions, our enantiomeric amino acid profiling revealed low plasma L-serine and high
448 urinary L-serine (Figure supplements 1B, 2B). Additionally, the proteomics analysis indicated
449 a reduction in B^0AT3 levels (4h IRI/sham = 0.56 fold; 8h IRI/sham = 0.65 fold; Table S1).
450 These observations suggest that the low L-serine reabsorption in IRI is a result of B^0AT3
451 reduction.

452 In proteomics, some transporters including ASCT2 were found to be increased in the
453 AKI conditions (Figure 2B), yet the mechanism behind this change is still unclear. snRNA-seq
454 study revealed that the cell clusters in all proximal tubular segments during early AKI were
455 drastically different from the healthy kidney suggesting that the new distinct cell clusters in
456 AKI were *de novo* synthesized for the repair process, as early AKI is a reversible condition

457 (Kirita et al., 2020). ASCT2 was found to be only one type of small amino acid transporter
458 which was increased during AKI conditions (Figure 2B). ASCT2 was reported to be highly
459 expressed in proliferative cells and stem cells and played a key role in the regulation of
460 mammalian target of rapamycin (mTOR) signaling pathway and glutamine-mediated
461 metabolism (Formisano and Van Winkle, 2016; Kandasamy et al., 2018; Scalise et al., 2018).
462 We postulate that ASCT2 is a nascent transporter to provide small amino acids and glutamine
463 for cell growth, as a molecular mechanism in *de novo* cellular synthesis for the recovery
464 processes.

465 Besides ASCT2 and SMCTs, other transporters may contribute to D-serine handling in
466 the kidney. Influxes of D-[^{3}H]serine in the Na^+-free condition of the normal mouse BBMVs
467 accounted for ~ 30% of total uptake (Figure 7A-B). These are results of the experimental
468 background of non-specific accumulation of radiotracers and probably also Na^+-independent
469 transporter(s). In BBMVs from 8h IRI model, D-[^{3}H]serine uptake without preloading
470 suggested the existence of Na^+-dependent transporters during the injury. In the D-serine
471 transporter screening, we found that PAT1 and B^0AT3 attenuated D-serine-mediated growth
472 inhibition (Figure 4C-D). PAT1 is reported to transport D-serine in the transfected cell and
473 oocyte models while the recognition of D-serine by B^0AT3 is unknown (Boll et al., 2002; Chen
474 et al., 2003). PAT1, a low-affinity proton-coupled amino acid transporter (K_m in mM range),
475 has been found at both sub-apical membranes of the S1 segment and inside of the epithelia
476 (The Human Protein Atlas: https://www.proteinatlas.org; updated on Dec 7th, 2022) (Sagné et
477 al., 2001; Vanslambrouck et al., 2010). PAT1 exhibits optimum function at pH 5 - 6 but very
478 low activity at pH 7 (Miyauchi et al., 2005; Bröer, 2008b). Future research is required to
479 address the significance of PAT1 on D-serine transport in the proximal tubule segments where
480 pH regulation is known to be highly dynamic (Boron, 2006; Nakanishi et al., 2012; Bouchard
481 and Mehta, 2022; Imenez Silva and Mohebbi, 2022). Despite the D-serine transport systems at

482 the apical side, other transport systems at the basolateral side are also necessary to complete
483 the picture of the D-serine transport systems in renal proximal tubules.

484 Transport of a micromolecule is contributed by multiple transporters that orchestrate
485 together to maintain homeostasis and to control transport compensation in an aberrant
486 condition (Bröer et al., 2016; Wiriyasermkul et al., 2020; Gauthier-Coles et al., 2021;
487 Sakaguchi et al., 2024). The molecular characteristics and physiological functions of
488 transporters are largely dependent on their microenvironments, such as electrochemical
489 gradients and the presence of other transporters for coordinating functions. In our proteomic
490 analysis, a high population of membrane transport proteins was obtained in the dataset by
491 applying urea treatment to the membrane preparation process (Figure 2, Table supplement 1)
492 (Kongpracha et al., 2022). By integrating data focused on specific targets, such as transporters
493 or amino acids, from the protein molecule level to the metabolome or proteome, we were able
494 to reveal the subtle changes in the body and identify the causes of those small changes. This
495 integrative and multi-hierarchical approach, emphasizing the coordinate functions of multiple
496 transporters, holds the potential for investigating the dynamics of a broad range of
497 micromolecules under diverse or intricate conditions within any tissues or organs.

498 # Materials and Methods

499 **Materials, animals, and graphical analysis**

500 General chemicals and cell culture media were purchased from Wako Fujifilm and
501 Nacalai tesque. Chemicals used in mass spectrometry were HPLC or MS grades. Flp-In T-Rex
502 293 cells, Expi293F cells, Expi293 Expression medium, Lipofectamine 3000, fluorescent-
503 labeled secondary antibodies, and Tyramide SuperBoost kit were from Thermo. Amino acids,
504 fetal bovine serum (FBS), anti-FLAG antibody, and anti-FLAG M2 column were from Sigma.
505 Secondary antibodies with HRP conjugated were from Jackson ImmunoResearch. L-
506 [^{3}H]Serine, D-[^{3}H]serine, L-[^{3}H]alanine, and D-[^{3}H]alanine were from Moravek. L-
507 [^{3}H]Glutamic acid, D-[^{3}H]glutamic acid, L-[^{14}C]tyrosine, D-[^{14}C]tyrosine, DL-[^{3}H]lactic acid,
508 [^{3}H]propionic acid, [^{14}C]nicotinic acid, [^{14}C]uric acid, and L-[^{3}H]aspartic acid were from
509 American Radiolabeled Chemicals. Anti-SGLT2 (SC-393350) and anti-Na^{+}/K^{+}-ATPase (SC-
510 21712) antibodies were obtained from Santa Cruz Biotechnology.

511 All animal experiments were carried out following institutional guidelines under the
512 approval of the Animal Experiment Committees of The Jikei University School of Medicine,
513 Nara Medical University, and Keio University, Japan. Eight weeks old C57BL/6J mice were
514 purchased from Japan SLC and CLEA Japan. Frozen kidneys of the 8 weeks old C57BL/6J
515 mice were purchased from Sankyo Labo Service.

516 Human genes/proteins were defined with all letters in uppercase while those of the
517 mouse molecules were defined with the first letter in uppercase. Unless otherwise indicated,
518 data shown in all figures are mean ± SEM of the representative data from 3 reproducible
519 experiments. Statistical differences and p-values were determined using the unpaired Student *t*
520 test. Graphs, statistical significance, and kinetics were analyzed and plotted by GraphPad Prism
521 8.4.

522 **Plasmid construction**

523 In this study, we used the cDNA of human SLC5A8/SMCT1 clone "NM_145913". We
524 generated the clone NM_145913 from the clone AK313788 (NBRC, NITE, Kisarazu, Japan).
525 At first, SMCT1 from AK313788 was subcloned into p3XFLAG-CMV14 (Sigma) via *Hind*III
526 and *Bam*HI sites. The clone "pCMV14-SMCT1" NM_145913 was subsequently generated by
527 mutagenesis of p3XFLAG-CMV14-SMCT1_AK313788 at I193V, T201A and I490M
528 (variants between NM_145913 and AK313788) by HiFi DNA Assembly Cloning (NEB) and
529 site-directed mutagenesis. Human SLC5A12/SMCT2 cDNA (NM_178498; Sino Biological
530 Inc.) was amplified by PCR and cloned into p3XFLAG-CMV14 via *Kpn*I and *Bam*HI sites to
531 generate "pCMV14-SMCT2". Human expression clones of SLC7A10/Asc-1 (NM_019849),
532 SLC7A1/CAT1 (NM_003045), SLC36A1/PAT1 (NM_078483), SLC2A5/GLUT5
533 (NM_003039), SLCO4C1/OATP-H (NM_180991), SLC22A13/OAT10 (NM_004256),
534 SLC22A7/OAT2 (NM_153320), SLC6A18/B^0AT3 (NM_182632), SLC15A2/PEPT2
535 (NM_021082), and TMEM27/Collectrin (NM_020665) were obtained from GenScript and
536 RIKEN BRC through the National BioResource Project of the MEXT/AMED, Japan. Mouse
537 Asct2 (NM_009201) TrueORF clone was obtained from OriGene. p3XFLAG-CMV14 empty
538 vector was used for Mock production. pcDNA5-SMCT1 and pcDNA5-SMCT2 used for
539 generation of SMCT1- and SMCT2-stable cell lines, respectively, were constructed by
540 assembling the PCR products of SMCT1 or SMCT2 into pcDNA5/FRT/TO (Thermo) by HiFi
541 DNA Assembly Cloning.

542 **Antibody (Ab) production**

543 Anti-mouse Smct1 Ab was custom-produced. Peptide antigen corresponding to the
544 amino acid residues 596 – 611 of Smct1 and the corresponding anti-sera from the immunized
545 rabbit was produced by Cosmo Bio. Anti-Smct1 Ab was purified using HiTrap Protein G HP

546 (GE Healthcare) following the manufacturer's protocol. After purification, the Ab was dialyzed
547 against PBS pH 7.4 and adjusted concentration to 1 mg/mL.

548 Anti-human ASCT2 and anti-mouse Asct2 Abs were custom-produced. First, we
549 generated pET47b(+)-GST vector by subcloning the GST from pET49b(+) template into
550 pET47b(+) via *Not*I and *Xho*I restriction sites. Then, human ASCT2 antigen (amino acid
551 residues 7 – 20) was amplified and cloned into pET47b(+)-GST to obtain GST-fused ASCT2
552 antigen. For the Asct2 antigen, both N-terminal (Asct2(NT), amino acid residues 1 – 38) and
553 C-terminal (Asct2(CT), amino acid residues 521 – 553) fragments were fused with GST by
554 cloning into pET47b(+)-GST and pET49b(+), respectively (Cosmo Bio). The GST-fusion
555 antigens were expressed in *E. coli* BL21(DE3) and purified by Glutathione Sepharose 4B (GE
556 Healthcare) as described previously (Nagamori et al., 2016a). The antigens were used to
557 immunize rabbits to obtain anti-sera (Cosmo Bio).

558 Anti-ASCT2 Ab was purified from the anti-sera using HiTrap Protein G HP (GE
559 Healthcare) following the manufacturer's protocol. After purification, the Ab was dialyzed
560 against PBS pH 7.4 and adjusted concentration to 1 mg/mL.

561 Anti-Asct2(NT) and anti-Asct2(CT) Abs were purified by using two-step purifications.
562 First, affinity columns of GST-fused Asct2(NT)-antigen and GST-fused Asct2(CT)-antigen
563 were produced by conjugating the antigens with HiTrap NHS-activated HP (GE Healthcare).
564 To purify anti-Asct2(NT) Ab, the anti-sera was subjected to the first purification by using the
565 GST-fused Asct2(NT)-antigen column. The elution fraction was dialyzed and subsequently
566 subjected to the second column of GST-fused Asct2(CT)-antigen column. The flowthrough
567 fraction corresponding to the affinity-purified anti-Asct2(NT) Ab was obtained. Purification of
568 anti-Asct2(CT) Ab was performed in the same way as Asct2(NT) Ab but used GST-fused
569 Asct2(CT)-antigen column followed by GST-fused Asct2(NT)-antigen column.

570 **Ischemia-reperfusion injury (IRI) model**

571 C57BL/6J (CLEA Japan) male mice between 12 – 16 weeks old underwent
572 experimental procedures for the IRI model. Ischemia-reperfusion was performed as previously
573 described (Sasabe et al., 2014). Before IRI induction, right kidney was removed. After twelve
574 days, the mice were grouped by randomization. Ischemia was operated for 45 min by clamping
575 the vessel under anesthesia. After that, the vessel clamp was removed, and the abdomen was
576 closed. Sham-operated control mice were treated identically except for clamping. Urine and
577 blood samples were collected at 4, 8, 20 and 40 hours after reperfusion. The mice were
578 anesthetized with isoflurane and euthanized by perfusion with PBS pH 7.4. The kidney was
579 removed and stored at -80 °C until use.

580 **Measurement of amino acid enantiomers by 2D-HPLC**

581 Plasma and urine samples collected from IRI mice were prepared as described with
582 modifications (Miyoshi et al., 2009; Hamase et al., 2010). Briefly, 20-fold volumes of methanol
583 were added to the samples and an aliquot was placed in a brown shading tube and used for
584 NBD derivatization (1 μL of the plasma was used for the reaction). After drying the solution
585 under reduced pressure, 20 μL of 200 mM sodium borate buffer (pH 8.0) and 5 μL of
586 fluorescent-labeling reagent [40 mM 4-fluoro-7-nitro-2,1,3-benzoxadiazole (NBD-F) in
587 anhydrous acetonitrile (MeCN)] were added, and then heated at 60 °C for 2 min. An aqueous
588 0.1% (v/v) TFA solution (375 μL) was added, and 20 μL of the reaction mixture was applied
589 to 2D-HPLC.

590 Enantiomers of amino acids were quantified using the 2D-HPLC platform (Miyoshi et
591 al., 2009; Hamase et al., 2010). The NBD-derivatives of the amino acids were separated using
592 a reversed-phase column (Singularity RP column, 1.0 mm i.d. × 50 mm; designed by Kyushu
593 University and KAGAMI INC.) with the gradient elution using aqueous mobile phases
594 containing MeCN and formic acid. To determine D- and L-amino acids, the fractions of amino

595 acids were automatically collected using a multi-loop valve and transferred to the
596 enantioselective column (Singularity CSP-001S, 1.5 mm i.d. × 75 mm; designed by Kyushu
597 University and KAGAMI INC.). Then, D- and L-amino acids were separated in the second
598 dimension by the enantioselective column. The mobile phases are the mixed solutions of
599 MeOH–MeCN containing formic acid, and the fluorescence detection of the NBD-amino acids
600 was carried out at 530 nm with excitation at 470 nm. Target peaks were quantified by scaling
601 the standard peak shapes (Hamase et al., 2018).

602 **Isolation of brush border membrane vesicles (BBMVs) for mass spectrometry analysis**

603 BBMVs were prepared by the calcium precipitation method (Biber et al., 2007;
604 Kongpracha et al., 2022). Frozen kidneys were minced into fine powders by using a polytron-
605 type homogenizer (Physcotron, Microtec) in the homogenization buffer containing 20 mM
606 Tris-HCl, pH 7.6, 250 mM sucrose, 1 mM EDTA and cOmplete EDTA-free protease inhibitor
607 cocktail (Roche). After low-speed centrifugation at 1,000 ×g and 3,000 ×g, the supernatant was
608 collected and incubated with 11 mM $CaCl_2$ for 20 min on ice with mild shaking. The
609 supernatant was ultra-centrifuged at 463,000 ×g for 15 min at 4 °C. The pellet was resuspended
610 in the homogenization buffer and repeated the steps of $CaCl_2$ precipitation. Finally, the pellet
611 of BBMVs was resuspended in 20 mM Tris-HCl pH 7.6, and 250 mM sucrose. Membrane
612 proteins of BBMVs were enriched by the Urea Wash method (Kongpracha et al., 2022). The
613 urea-washed BBMV samples were subjected to sample preparation for mass spectrometry.

614 **Cell culture, transfection, and generation of stable cell lines**

615 HEK293 and Flp-In T-Rex 293 cells were cultured in DMEM supplemented with 10 %
616 (v/v) FBS, 100 units/mL penicillin G, and 100 μg/mL streptomycin (P/S), and routinely
617 maintained at 37 °C, 5 % CO_2 and humidity. For transfection experiments, the cells were
618 seeded in antibiotic-free media for one day prior to transfection to obtain approximately 40%

619 confluence. DNA transient transfection and ASCT2-siRNA (ID#s12916; Ambion) transfection
620 were performed by using Lipofectamine 3000 following the manufacturer's protocol. The ratio
621 of DNA : P3000 : Lipofectamine 3000 is 1.0 μg : 2.0 μL : 1.5 μL. The ratio of siRNA :
622 Lipofectamine 3000 is 10 pmol : 1 μL. The cells were further maintained in the same media
623 for two days prior to the assays.

624 Flp-In T-REx 293 stably expressing SMCT1 (FlpInTR-SMCT1) and SMCT2
625 (FlpInTR-SMCT2) were generated by co-transfection of pOG44 and pcDNA5-SMCT1 or
626 pcDNA5-SMCT2 and subsequently cultured in the media containing 5 mg/L blasticidin and
627 150 mg/L hygromycin B for positive clone selection. Mock cells were generated in the same
628 way using the empty plasmid. Expressions of SMCT1 in FlpInTR-SMCT1 and SMCT2 in
629 FlpInTR-SMCT2 were induced by adding 1 mg/L doxycycline hyclate (Dox; Tet-ON system)
630 at one day after seeding. The cells were further cultured for two days prior to performing
631 experiments.

632 Wild-type and *ASCT2*-knockout HAP1 cells (Human near-haploid cell line; Horizon
633 Discovery) were cultured in IMDM supplemented with 10 % (v/v) FBS, P/S, and routinely
634 maintained at 37 °C, 5 % CO_2 and humidity.

635 Expi293F cells were cultured in Expi293 Expression medium at 37 °C, 8 % CO_2, and
636 humidity. To express SMCT1 transiently, the cells were transfected with pCMV14-SMCT1
637 using PEI MAX pH 6.9 (MW 40,000; Polysciences) and cultured for two days.

638 **Mass spectrometry and proteome data analysis**

639 Proteomics of mouse BBMVs was analyzed as described (Uetsuka et al., 2015;
640 Kongpracha et al., 2022). After preparing urea-washed BBMVs, the samples were fractionated
641 into four fractions by SDB-XC StageTips and desalted by C18-StageTips. Mass spectrometry
642 was performed using the Q Exactive (Thermo) coupled with nano-Advance UHPLC (Michrom
643 Bioresources). The UHPLC apparatus was equipped with a trap column (L-column ODS, 0.3

644 x 5 mm, CERI) and a C18 packed tip column (0.1 x 125 mm; Nikkyo Technos). Raw data from
645 four fractions were analyzed using Proteome Discoverer 2.2 (Thermo) and Mascot 2.6.2
646 (Matrix Science). Data from four fractions were combined and searched for identified proteins
647 from the UniProt mouse database (released in March 2019). The maximum number of missed
648 cleavages, precursor mass tolerance, and fragment mass tolerance were set to 3, 10 ppm and
649 0.01 Da, respectively. The carbamidomethylation Cys was set as a fixed modification.
650 Oxidation of Met and deamidation of Asn and Gln were set as variable modifications. A filter
651 (false discovery rate < 1%) was applied to the resulting data. For each mouse sample, the
652 analysis was conducted twice and the average was used. One data set was composed of 3
653 samples from each operation condition (n = 3). Statistical analyses were determined using
654 Proteome Discoverer 2.2 (Thermo). Statistical differences and p-values were determined using
655 the unpaired Student *t* test. Data represented the median ± SEM (Table S1).

656 Mass spectrometry of HEK293 cells was analyzed from crude membrane fractions.
657 Membrane fractions from HEK293 cells were prepared from 3-day cultured cells as described
658 (Nagamori et al., 2016b). Membrane proteins were enriched by the Urea Wash method, and
659 tryptic peptides were subject for analysis as described above.

660 Proteome of BBMVs from mouse kidneys after ischemia operation for 4 (4h) or 8 hours
661 (8h) was normalized to that of sham operation. The identified proteins were then subjected to
662 annotate the biological functions by Ingenuity Pathway Analysis (IPA, Qiagen). Molecules
663 from the dataset that met the cutoff of the Ingenuity Knowledge Base were considered for the
664 analysis. A right-tailed Fisher's Exact Test was used to calculate the p-value determining the
665 probability (z-scores) of the biological function. Protein localization in kidney segments was
666 evaluated based on related literature and The Human Protein Atlas
667 (http://www.proteinatlas.org: updated Dec 7th, 2022).

668 **Effect of D-serine on cell growth**

669 HEK293 cells were seeded into 96-well-plate at 10,000 cells/well. Transient
670 transfection was performed 12 hours after seeding followed by L- or D-serine treatment at 12
671 hours after that. In the case of FlpInTR-stable cell lines, if needed, ASCT2 siRNA was
672 transfected 12 hours after seeding. Dox was added one day after seeding followed by treatment
673 with L- or D-serine (in the presence or absence of ibuprofen as indicated) 10 hours after adding
674 Dox. The cells were further maintained for two days. Cell growth was examined by XTT assay.
675 In one reaction, 50 μL of 1 mg/mL XTT (2,3-Bis-(2-Methoxy-4-Nitro-5-Sulfophenyl)-2*H*-
676 Tetrazolium-5-Carboxanilide) (Biotium) was mixed with 5 μL of 1.5 mg/mL phenazine
677 methosulfate. The mixture was applied to the cells and incubated for 4 hours at 37 °C in the
678 cell culture incubator. Cell viability was evaluated by measuring the absorbance at 450 nm.
679 Cell growth in serine treatment samples was compared to the control (without serine treatment).
680 For transporter screening, the growth of the transfected cells at a specific D-serine concentration
681 was compared to that of Mock after normalization with no treatment.

682 **Transport assay in cultured cells**

683 Transport assay in cells was performed as described previously with some
684 modifications (Wiriyasermkul et al., 2012). Briefly, for D-[^{3}H]serine transport in HEK293
685 cells, the cells were seeded into poly-D-lysine-coated 24-well plates at 1.2 x 10^5 cells/well and
686 cultured for three days. Unless indicated elsewhere, uptake of 20 μM (100 Ci/mol) or 100 μM
687 (10 Ci/mol) D-[^{3}H]serine was measured in PBS pH 7.4 at 37 °C at the indicated time points.
688 After termination of the assay, the cells were lysed. An aliquot was subjected to measure
689 protein concentration, and the remaining lysate was mixed with Optiphase HiSafe 3
690 (PerkinElmer). The radioactivity was monitored using a β-scintillation counter (LSC-8000,
691 Hitachi). In the transport assay with or without Na^+, Na^+-HBSS, or Na^+-free HBSS (choline-
692 Cl substitution) were used instead of PBS.

693 Transport assay in FlpInTR-stable cell lines was performed in a similar way to HEK293
694 cells. After cell seeding for one day, SMCT1 and SMCT2 expression were induced by adding
695 Dox for two days. For the ASCT2 knockdown experiment, ASCT2-siRNA was transfected 12
696 hours prior to Dox induction. The time course of 100 μM D-[^{3}H]serine transport (10 Ci/mol)
697 was measured 37 °C for 5 – 20 min. Inhibition assay was performed by adding the inhibitors
698 at the same time with D-[^{3}H]serine substrate. Kinetics of D-[^{3}H]serine transport were examined
699 by the uptake of D-[^{3}H]serine at the concentration of 0.5 – 8 mM (0.125 – 2 Ci/mol) for 10 min
700 at 37 °C.

701 Transport of D-[^{3}H]serine in wild-type and *ASCT2*-knockout HAP1 was performed in
702 a similar way to HEK293 and FlpInTR-stable cells but without the process of transfection.

703 **SMCT1 purification, proteoliposome reconstitution, and transport assay**

704 Human SMCT1 was purified from SMCT1-expressing Expi293F cells. Membrane
705 fraction and purification processes were performed as previously described with small
706 modifications (Nagamori et al., 2016a). First, cell pellets were resuspended in 20 mM Tris-HCl
707 pH 7.4, 150 mM NaCl, 10% (v/v) glycerol, and protease inhibitor cocktail (Roche). The crude
708 membrane fraction was derived from sonication and ultracentrifugation (sonication method).
709 Membrane proteins were extracted from the crude membrane fraction with 2% (w/v) DDM
710 and ultracentrifugation. SMCT1 was purified by anti-FLAG M2 affinity column. Unbound
711 proteins were washed out by 20 mM Tris-HCl pH 7.4, 200 mM NaCl, 10% (v/v) glycerol, and
712 0.05% (w/v) DDM. Then SMCT1 was eluted by 3xFLAG peptide in the washing buffer.
713 Purified SMCT1 was concentrated by Amicon Ultra Centrifugal Filters 30K (Millipore).

714 The reconstitution of proteoliposomes was performed as described with minor
715 modifications (Lee et al., 2019). The purified SMCT1 was reconstituted in liposomes (made
716 from 5:1 (w/w) of type II-S PC : brain total lipid) at a protein-to-lipid ratio of 1:100 (w/w) in
717 20 mM MOPS-Tris pH 7.0 and 100 mM KCl.

718 Transport assay in proteoliposomes was conducted by the rapid filtration method (Lee
719 et al., 2019). Uptake reaction was conducted by dilution of 1 μg SMCT1 proteoliposomes in
720 100 μL uptake buffer (20 mM MOPS-Tris pH 7.0, 100 mM NaCl for Na^+-buffer or KCl for
721 Na^+-free buffer, 1 mM $MgSO_4$ and 1 mM $CaCl_2$) containing radioisotope-labeled substrates.
722 The reaction was incubated at 25 °C for an indicated time. The radioisotope-labeled substrates
723 were used as follows: 5 Ci/mol for [^{14}C]uric acid, L-[^{14}C]tyrosine and D-[^{14}C]tyrosine; 10
724 Ci/mol for DL-[^{3}H]lactic acid, L-[^{3}H]alanine, D-[^{3}H]alanine, L-[^{3}H]serine, D-[^{3}H]serine, L-
725 [^{3}H]glutamic acid and D-[^{3}H]glutamic acid; and 20 Ci/mol for [^{3}H]propionic acid. In the
726 inhibition assay, 1 mM ibuprofen was applied at the same time with the radioisotope-labeled
727 substrates. Kinetics of nicotinate transport were measured for 3 min using 0.01 – 2 mM
728 [^{14}C]nicotinate (0.2 – 50 Ci/mol) in Na^+-containing buffer, and then subtracted from the uptake
729 in Na^+-free buffer.

730 **Transport assay in mouse BBMVs**

731 Both left and right kidneys from eight weeks old male normal control (Japan SLC;
732 Sankyo Labo Service) or IRI model (sham, 4h IRI, and 8h IRI) were taken out after PBS
733 perfusion and frozen until use. After mincing and homogenizing the frozen kidneys in the
734 buffer containing 20 mM Tris-HCl pH 7.6, 150 mM mannitol, 100 mM KCl, 1 mM EDTA,
735 and protease inhibitor cocktail, the BBMVs were prepared as described in the above section
736 but using magnesium instead of calcium for BBMV precipitation. The pellet of BBMVs was
737 resuspended in the suspension buffer (10 mM Tris-HCl, pH 7.6, 100 mM mannitol, and 100
738 mM KCl). In the L-glutamine preloading experiment, the BBMVs were incubated with 4 mM
739 L-glutamine (L-Gln) or only buffer (no preload) on ice for 3 hours. External buffers were then
740 removed by centrifugation at 21,000 ×*g* for 20 min and the BBMVs were resuspended in the
741 suspension buffer.

742 Transport assay was performed by rapid filtration. Prior to initiating the reaction, 5 μM
743 valinomycin was added to the BBMV samples. Transport assay was examined by diluting 100
744 μg BBMVs in 100 μL of the uptake buffer (10 mM Tris-HCl pH 7.6, 150 mM NaCl for Na^+
745 condition or KCl for Na^+-free condition, 50 mM mannitol and 5 μM valinomycin) containing
746 radioisotope substrates, 10 μM D-[^{3}H]serine (100 Ci/mol) or 10 μM L-[^{3}H]aspartic acid (100
747 Ci/mol), as described in the figures. The reaction was incubated at 30 °C at an indicated time,
748 then terminated by the addition of ice-cold buffer containing 10 mM Tris-HCl pH 7.6 and 200
749 mM mannitol and filtered through 0.45 μm nitrocellulose filter (Millipore), followed by
750 washing with the same buffer once. The membranes were soaked in Clear-sol I (Nacalai
751 Tesque), and the radioactivity on the membrane was monitored. For the inhibition experiments,
752 the tested inhibitors were added into the D-[^{3}H]serine substrate solution at the same time.

753 **Western Blot analysis**

754 Expressions of targeting proteins from membrane fractions were verified by Western
755 blot analysis as described (Nagamori et al., 2016b). Membrane fractions were dissolved in 1%
756 w/v DDM prior to the addition of the SDS-PAGE sample buffer. Signals of chemiluminescence
757 (Immobilon Forte Western HRP substrate; Millipore) were visualized by ChemiDoc MP
758 Imaging system (Bio-Rad).

759 **Immunofluorescence staining of mouse kidneys**

760 The 8 weeks old male C57BL/6J mice (Japan SLC) were anesthetized and fixed by
761 anterograde perfusion via the aorta with 4% w/v paraformaldehyde in 0.1 M sodium phosphate
762 buffer pH 7.4. The kidneys were dissected, post-fixed in the same buffer for two days, and
763 cryoprotected in 10 %, 20 %, and 30 % w/v sucrose. Frozen kidney sections were cut at 7 μm
764 thickness in a cryostat (Leica) and mounted on MAS-coated glass slides (Matsunami). The
765 sections were placed in antigen retrieval buffer (10 mM citrate and 10 mM sodium Citrate),

766 autoclaved at 121 °C for 5 min and washed by TBS-T (Tris-buffered saline (TBS) with 0.1 %
767 v/v Tween 20). Immunostaining was done by serial incubation with each antibody as below.

768 For Asct2 and Sglt2 co-immunostaining, the samples were incubated with 3 %
769 hydrogen peroxide solution for 10 min, washed with TBS, and incubated in Blocking One
770 Histo (Nacalai tesque) for 15 min. The samples were then incubated with mouse anti-SGLT2
771 antibody diluted in immunoreaction enhancer B solution (Can Get Signal immunostain,
772 TOYOBO) overnight at 4 °C. Signal was enhanced by Alexa Fluor 568 Tyramide SuperBoost
773 (TSA) kit, goat anti-mouse IgG, following the manufacturer's instruction (Thermo). The
774 antibodies were then stripped by citrate/acetate-based buffer, pH 6.0, containing 0.3% w/v SDS
775 at 95 °C for 10 min (Buchwalow et al., 2018), washed by TBS, and incubated with Blocking
776 One Histo. Asct2 staining was done as described (Nagamori et al., 2016a). Briefly, the samples
777 were incubated with rabbit anti-Asct2(NT) antibody diluted in immunoreaction enhancer A
778 solution (Can Get Signal immunostain) overnight at 4 °C. After washing with TBS-T, the
779 specimens were incubated with Alexa Fluor 488-labeled donkey anti-rabbit IgG.

780 For Asct2 and Agt1 co-immunostaining, signals of both antibodies were enhanced by
781 TSA kit. First, the specimens were incubated with rabbit anti-Agt1(G) antibody (Nagamori et
782 al., 2016a) overnight at 4 °C followed by Alexa Fluor 568 TSA kit with goat anti-rabbit. The
783 antibodies were then stripped. The specimens were incubated with rabbit anti-Asct2(NT)
784 overnight at 4 °C and then repeated the steps of TSA kit using Alexa Fluor 488, goat anti-
785 rabbit.

786 Staining of Asct2 and Na^+/K^+-ATPase was performed without TSA enhancement. After
787 blocking by Blocking One Histo, the samples were incubated with rabbit anti-Asct2(NT)
788 antibody diluted in immunoreaction enhancer A solution overnight. The samples were washed
789 with TBS-T, incubated with Alexa Fluor488-labeled donkey anti-rabbit IgG, and washed again.
790 Non-specific staining was blocked by Blocking One Histo and the specimens were then

791 incubated with mouse anti-Na^+/K^+-ATPase antibody diluted in immunoreaction enhancer B
792 solution overnight at 4 °C. The specimens were washed with TBS-T and incubated with Alexa
793 Fluor568-labeled goat anti-mouse IgG for 1 hour.

794 Smct1 and Sglt2 were co-stained. After blocking by Blocking One Histo, the samples
795 were incubated with rabbit anti-Smct1 antibody and mouse anti-SGLT2 diluted in
796 immunoreaction enhancer B solution overnight at 4 °C. The specimens were washed with TBS-
797 T and incubated with Alexa Fluor488-labeled donkey anti-rabbit IgG and Alexa Fluor568-
798 labeled goat anti-mouse IgG for 1 hour.

799 Prior to the co-staining of Smct1 and Agt1, anti-Agt1 antibody was conjugated with
800 Alexa Fluor 568 dye via succinimidyl ester reaction. The antibody was adjusted to pH 8.3 and
801 mixed with Alexa Fluor 568 NHS Ester (Thermo) for 2 hours. The reaction was stopped by
802 incubation with 1 M ethanolamine for 1 hour. The unconjugated dye was removed by size
803 exclusion using Bio-Spin P-30 gel columns (Bio-rad) equilibrated in PBS pH 7.4. For Smct1
804 and Agt1 co-staining, after the blocking step, the samples were firstly stained with rabbit anti-
805 Smct1 antibody diluted in immunoreaction enhancer A solution. Signal was enhanced by Alexa
806 Fluor 488 TSA kit with goat anti-rabbit IgG. Subsequently, the specimen was washed with
807 TBS-T and non-specific staining was blocked by Blocking One Histo. The samples were then
808 incubated with Alexa Fluor 568-conjugated anti-Smct1 antibody diluted in Blocking One Histo
809 overnight at 4 °C.

810 All specimens were washed with TBS-T and mounted with Fluoromount (Diagnostic
811 Biosystems). Imaging was detected using a KEYENCE BZ-X710 microscope. Images were
812 color-adjusted using ImageJ ver. 1.51 (NIH). Images in Figure 3B were subjected to
813 deconvolution process in Fiji/ImageJ2 ver. 2.9 prior to color adjustment.

814 **Analysis of Smcts and Asct2 from the open-sourced dataset of single nucleus RNA**
815 **sequencing (snRNA-seq) of the IRI model**

816 The dataset of snRNA-seq used is created from the mice after ischemia-reperfusion
817 injury (IRI) and published by Kirita et al. (Kirita et al., 2020). The snRNA-seq dataset
818 (GSE139107), which has already processed by zUMIs and SoupX, was downloaded from
819 GEO, a public functional genomics data repository (Barrett et al., 2012). The dataset revealed
820 percentage of mitochondrial UMI counts of each cell (calculated by *PercentageFeatureSet*
821 function of Seurat) to be < 0.01 % in more than 94% cells in each cluster. From the
822 "GSE139107_MouseIRI.metadata", we annotated the expression of Smct1, Smct2 and Asct2
823 in proximal tubule segments 1 – 3 (S1, S2, and S3) at the early stages of IRI (4 and 12 hours)
824 compared to the control mice. Downstream analyses including normalization, scaling and
825 visualization were performed by Seurat v3.2, an R package designed for Quality Control,
826 analysis and exploration of single-cell RNA-seq data (Stuart et al., 2019). After selecting the
827 cells in S1, S2, and S3 from the datasets (control, 4-hour IRI, and 12-hour IRI), we merged the
828 data of the cells in the same cluster. The data were then calculated as log-normalized values by
829 *NormalizeData* function and scaled by *ScaleData* function of Seurat. Visualization of the
830 expression data was performed using Seurat plug-in of R software and ggplot2 plug-in of R
831 software (Wickham, 2010). Dot plots of gene expression in each cluster after log-
832 transformation and scaling were created by *Dotplot* function of Seurat.

833 **Data and materials availability**

834 All proteomics data have been deposited in Japan Proteome Standard Repository/Database:
835 JPST000929 and JPST000931. Codes for snRNA sequencing reanalysis are available in
836 GitHub repository at https://github.com/SN-PW/snRNA_seq.git.

Acknowledgments

We greatly appreciate Noriyoshi Isozumi for preliminary proteomic analysis, Yuki Mori, Junko Iwatani, and Yuika Shimo for experimental assistance, Hiroshi Imoto, Eiichi Negishi, Maiko Nakane, and Shoto Ishigo for optimization of enantiomeric amino acid analysis, Genro Kashino and Haruka Minowa for management of radioisotope facilities, Rikako Furuya for crucial discussion, Xuan Trang T Nguyen for her native English proofreading, and Sae Ochi and Tomokazu Matsuura for their tremendous supports. We are especially grateful to Yoshinori Moriyama for his critical reading and suggestion. This work is partly supported by JSPS KAKENHI (JP22K06150) to P.W. and (JP21H03365) to S.N.; research grant from Takeda Science Foundation to P.W.; research grants from Gout and uric acid Foundation, Nakatani Foundation, Shiseido Company, Ltd., AMED (JP21ek0310012), and AMED-CREST (JP21gm0810010) to S.N.; and unrestricted fund provided from Dr. Jin and Mrs. Keiko Hanyu (Jiseikai Kajigaya Clinic.) to S.N. and P.W.

Competing Interest Statement

A patent (WO/2021/132691) has been applied by KAGAMI Inc., Nara Medical University, and NIBIOHN with P.W., S.M., P.K., T.K., M.Mit., and S.N. as inventors based on this research. M.Mit. is a founder and CEO of KAGAMI Inc., a startup company working on chiral amino acids analysis and research for medical applications. The authors declare no potential conflicts of interest.

Author contributions

Pattama Wiriyasermkul—Methodology, Investigation, Validation, Formal analysis, Data curation, Visualization, Funding acquisition, Writing—original draft, Writing—review and editing

Satomi Moriyama—Investigation, Formal analysis

Masataka Suzuki—Investigation, Formal analysis

Pornparn Kongpracha—Investigation, Formal analysis, Data curation

Nodoka Nakamae—Investigation

Saki Takeshita—Formal analysis, Data curation

Yoko Tanaka—Investigation

Akina Matsuda—Investigation

Masaki Miyasaka—Formal analysis, Validation

Kenji Hamase—Methodology, Investigation, Formal analysis

Tomonori Kimura—Methodology, Resources

Masashi Mita—Conceptualization, Funding acquisition

Jumpei Sasabe—Methodology, Investigation, Validation, Resources

Shushi Nagamori—Conceptualization, Methodology, Validation, Data curation, Supervision, Resources, Funding acquisition, Project administration, Writing—original draft, Writing—review and editing

All authors contributed to the final manuscript.

878 ## References

879 Avissar NE, Ryan CK, Ganapathy V, Sax HC. 2001. Na^+-dependent neutral amino acid
880 transporter ATB^0 is a rabbit epithelial cell brush-border protein. *American Journal of*
881 *Physiology-Cell Physiology* **281**:C963–C971. doi:10.1152/ajpcell.2001.281.3.C963

882 Bailey CG, Ryan RM, Thoeng AD, Ng C, King K, Vanslambrouck JM, Auray-Blais C,
883 Vandenberg RJ, Bröer S, Rasko JEJ. 2011. Loss-of-function mutations in the glutamate
884 transporter SLC1A1 cause human dicarboxylic aminoaciduria. *Journal of Clinical*
885 *Investigation* **121**:446–453. doi:10.1172/JCI44474

886 Barrett T, Wilhite SE, Ledoux P, Evangelista C, Kim IF, Tomashevsky M, Marshall KA,
887 Phillippy KH, Sherman PM, Holko M, Yefanov A, Lee H, Zhang N, Robertson CL,
888 Serova N, Davis S, Soboleva A. 2012. NCBI GEO: archive for functional genomics
889 data sets—update. *Nucleic Acids Research* **41**:D991–D995. doi:10.1093/nar/gks1193

890 Basu AC, Tsai GE, Ma C-L, Ehmsen JT, Mustafa AK, Han L, Jiang ZI, Benneyworth MA,
891 Froimowitz MP, Lange N, Snyder SH, Bergeron R, Coyle JT. 2009. Targeted disruption
892 of serine racemase affects glutamatergic neurotransmission and behavior. *Molecular*
893 *Psychiatry* **14**:719–727. doi:10.1038/mp.2008.130

894 Biber J, Stieger B, Stange G, Murer H. 2007. Isolation of renal proximal tubular brush-border
895 membranes. *Nature Protocols* **2**:1356–1359. doi:10.1038/nprot.2007.156

896 Bodner O, Radzishevsky I, Foltyn VN, Touitou A, Valenta AC, Rangel IF, Panizzutti R,
897 Kennedy RT, Billard JM, Wolosker H. 2020. D-Serine Signaling and NMDAR-
898 Mediated Synaptic Plasticity Are Regulated by System A-Type of Glutamine/D-Serine
899 Dual Transporters. *Journal of Neuroscience* **40**:6489–6502.
900 doi:10.1523/JNEUROSCI.0801-20.2020

901 Boll M, Foltz M, Rubio-Aliaga I, Kottra G, Daniel H. 2002. Functional Characterization of
902 Two Novel Mammalian Electrogenic Proton-dependent Amino Acid Cotransporters.
903 *Journal of Biological Chemistry* **277**:22966–22973. doi:10.1074/jbc.M200374200
904 Boron WF. 2006. Acid-Base Transport by the Renal Proximal Tubule. *Journal of the American*
905 *Society of Nephrology* **17**:2368-2382. doi: 10.1681/ASN.2006060620
906 Bouchard J, Mehta RL. 2022. Timing of Kidney Support Therapy in Acute Kidney Injury:
907 What Are We Waiting For? *American Journal of Kidney Diseases* **79**:417–426.
908 doi:10.1053/j.ajkd.2021.07.014
909 Bröer A, Rahimi F, Bröer S. 2016. Deletion of Amino Acid Transporter ASCT2 (SLC1A5)
910 Reveals an Essential Role for Transporters SNAT1 (SLC38A1) and SNAT2
911 (SLC38A2) to Sustain Glutaminolysis in Cancer Cells. *Journal of Biological Chemistry*
912 **291**:13194–13205. doi:10.1074/jbc.M115.700534
913 Bröer S. 2008a. Amino Acid Transport Across Mammalian Intestinal and Renal Epithelia.
914 *Physiological Reviews* **88**:249–286. doi:10.1152/physrev.00018.2006
915 Bröer S. 2008b. Apical Transporters for Neutral Amino Acids: Physiology and
916 Pathophysiology. *Physiology* **23**:95–103. doi:10.1152/physiol.00045.2007
917 Buchwalow I, Samoilova V, Boecker W, Tiemann M. 2018. Multiple immunolabeling with
918 antibodies from the same host species in combination with tyramide signal
919 amplification. *Acta Histochemica* **120**:405–411. doi:10.1016/j.acthis.2018.05.002
920 César-Razquin A, Snijder B, Frappier-Brinton T, Isserlin R, Gyimesi G, Bai X, Reithmeier RA,
921 Hepworth D, Hediger MA, Edwards AM, Superti-Furga G. 2015. A Call for Systematic
922 Research on Solute Carriers. *Cell* **162**:478–487. doi:10.1016/j.cell.2015.07.022
923 Chen Z, Fei Y, Anderson CMH, Wake KA, Miyauchi S, Huang W, Thwaites DT, Ganapathy
924 V. 2003. Structure, function and immunolocalization of a proton-coupled amino acid

925 transporter (hPAT1) in the human intestinal cell line Caco-2. *The Journal of Physiology*
926 **546**:349–361. doi:10.1113/jphysiol.2002.026500
927 Formisano TM, Van Winkle LJ. 2016. At Least Three Transporters Likely Mediate Threonine
928 Uptake Needed for Mouse Embryonic Stem Cell Proliferation. *Frontiers in Cell and*
929 *Developmental Biology* **4**. doi:10.3389/fcell.2016.00017
930 Foster AC, Farnsworth J, Lind GE, Li Y-X, Yang J-Y, Dang V, Penjwini M, Viswanath V,
931 Staubli U, Kavanaugh MP. 2016. D-Serine Is a Substrate for Neutral Amino Acid
932 Transporters ASCT1/SLC1A4 and ASCT2/SLC1A5, and Is Transported by Both
933 Subtypes in Rat Hippocampal Astrocyte Cultures. *PLoS ONE* **11**:e0156551.
934 doi:10.1371/journal.pone.0156551
935 Fu Y, Tang C, Cai J, Chen G, Zhang D, Dong Z. 2018. Rodent models of AKI-CKD transition.
936 *American Journal of Physiology-Renal Physiology* **315**:F1098–F1106.
937 doi:10.1152/ajprenal.00199.2018
938 Ganapathy V, Thangaraju M, Gopal E, Martin PM, Itagaki S, Miyauchi S, Prasad PD. 2008.
939 Sodium-coupled Monocarboxylate Transporters in Normal Tissues and in Cancer. *The*
940 *AAPS Journal* **10**:193. doi:10.1208/s12248-008-9022-y
941 Gauthier-Coles G, Vennitti J, Zhang Z, Comb WC, Xing S, Javed K, Bröer A, Bröer S. 2021.
942 Quantitative modelling of amino acid transport and homeostasis in mammalian cells.
943 *Nature Communications* **12**:5282. doi:10.1038/s41467-021-25563-x
944 Ghezzi C, Loo DDF, Wright EM. 2018. Physiology of renal glucose handling via SGLT1,
945 SGLT2 and GLUT2. *Diabetologia* **61**:2087–2097. doi:10.1007/s00125-018-4656-5
946 Gonda Y, Matsuda A, Adachi K, Ishii C, Suzuki M, Osaki A, Mita M, Nishizaki N, Ohtomo
947 Y, Shimizu T, Yasui M, Hamase K, Sasabe J. 2023. Mammals sustain amino acid
948 homochirality against chiral conversion by symbiotic microbes. *Proceedings of the*
949 *National Academy of Sciences USA* **120**:e2300817120. doi:10.1073/pnas.2300817120

950 Gopal E, Umapathy NS, Martin PM, Ananth S, Gnana-Prakasam JP, Becker H, Wagner CA,
951 Ganapathy V, Prasad PD. 2007. Cloning and functional characterization of human
952 SMCT2 (SLC5A12) and expression pattern of the transporter in kidney. *Biochimica et*
953 *Biophysica Acta (BBA) - Biomembranes* **1768**:2690–2697.
954 doi:10.1016/j.bbamem.2007.06.031
955 Hamase K, Miyoshi Y, Ueno K, Han H, Hirano J, Morikawa A, Mita M, Kaneko T, Lindner
956 W, Zaitsu K. 2010. Simultaneous determination of hydrophilic amino acid enantiomers
957 in mammalian tissues and physiological fluids applying a fully automated micro-two-
958 dimensional high-performance liquid chromatographic concept. *Journal of*
959 *Chromatography A* **1217**:1056–1062. doi:10.1016/j.chroma.2009.09.002
960 Hamase K, Ikeda T, Ishii C, Ishigo S, Masuyama K, Akita T, Furusho A, Takahashi M, Ide T,
961 Mita M. 2018. Determination of Trace Amounts of Chiral Amino Acids in Complicated
962 Biological Samples Using Two-Dimensional High-Performance Liquid
963 Chromatography with an Innovative "Shape-Fitting" Peak
964 Identification/Quantification Method. *CHROMATOGRAPHY* **39**:147–152.
965 doi:10.15583/jpchrom.2018.019
966 Hasegawa H, Masuda N, Natori H, Shinohara Y, Ichida K. 2019. Pharmacokinetics and
967 toxicokinetics of D-serine in rats. *Journal of Pharmaceutical and Biomedical Analysis*
968 **162**:264–271. doi:10.1016/j.jpba.2018.09.026
969 Hashimoto A, Nishikawa T, Hayashi T, Fujii N, Harada K, Oka T, Takahashi K. 1992. The
970 presence of free D-serine in rat brain. *FEBS Lett* **296**:33–36. doi:10.1016/0014-
971 5793(92)80397-y
972 Hesaka A, Sakai S, Hamase K, Ikeda T, Matsui R, Mita M, Horio M, Isaka Y, Kimura T. 2019.
973 D-Serine reflects kidney function and diseases. *Scientific Reports* **9**:5104.
974 doi:10.1038/s41598-019-41608-0

975 Imenez Silva PH, Mohebbi N. 2022. Kidney metabolism and acid–base control: back to the
976 basics. *Pflugers Arch - European Journal of Physiology* **474**:919–934.
977 doi:10.1007/s00424-022-02696-6
978 Itagaki S, Gopal E, Zhuang L, Fei Y-J, Miyauchi S, Prasad PD, Ganapathy V. 2006. Interaction
979 of Ibuprofen and Other Structurally Related NSAIDs with the Sodium-Coupled
980 Monocarboxylate Transporter SMCT1 (SLC5A8). *Pharmaceutical Research* **23**:1209–
981 1216. doi:10.1007/s11095-006-0023-1
982 Iwata Y, Nakade Y, Kitajima S, Yoneda-Nakagawa S, Oshima M, Sakai N, Ogura H, Sato K,
983 Toyama T, Yamamura Y, Miyagawa T, Yamazaki H, Hara A, Shimizu M, Furuichi K,
984 Mita M, Hamase K, Tanaka T, Nishida M, Muramatsu W, Yamamoto H, Shichino S,
985 Ueha S, Matsushima K, Wada T. 2022. Protective effect of D-alanine against acute
986 kidney injury. *American Journal of Physiology-Renal Physiology* **322**:F667–F679.
987 doi:10.1152/ajprenal.00198.2021
988 Kanai Y, Hediger MA. 1992. Primary structure and functional characterization of a high-
989 affinity glutamate transporter. *Nature* **360**:467–471. doi:10.1038/360467a0
990 Kandasamy P, Gyimesi G, Kanai Y, Hediger MA. 2018. Amino acid transporters revisited:
991 New views in health and disease. *Trends in Biochemical Sciences* **43**:752–789.
992 doi:10.1016/j.tibs.2018.05.003
993 Kaplan E, Zubedat S, Radzishevsky I, Valenta AC, Rechnitz O, Sason H, Sajrawi C, Bodner
994 O, Konno K, Esaki K, Derdikman D, Yoshikawa T, Watanabe M, Kennedy RT, Billard
995 J-M, Avital A, Wolosker H. 2018. ASCT1 (Slc1a4) transporter is a physiologic
996 regulator of brain D-serine and neurodevelopment. *Proceedings of the National*
997 *Academy of Sciences USA* **115**:9628–9633. doi:10.1073/pnas.1722677115
998 Kimura T, Hamase K, Miyoshi Y, Yamamoto R, Yasuda K, Mita M, Rakugi H, Hayashi T,
999 Isaka Y. 2016. Chiral amino acid metabolomics for novel biomarker screening in the

1000 prognosis of chronic kidney disease. *Scientific Reports* **6**:26137.
1001 doi:10.1038/srep26137
1002 Kimura T, Hesaka A, Isaka Y. 2020. Utility of D-serine monitoring in kidney disease.
1003 *Biochimica et Biophysica Acta (BBA) - Proteins and Proteomics* **1868**:140449.
1004 doi:10.1016/j.bbapap.2020.140449
1005 Kirita Y, Wu H, Uchimura K, Wilson PC, Humphreys BD. 2020. Cell profiling of mouse acute
1006 kidney injury reveals conserved cellular responses to injury. *Proceedings of the*
1007 *National Academy of Sciences USA* **117**:15874–15883. doi:10.1073/pnas.2005477117
1008 Kongpracha P, Wiriyasermkul P, Isozumi N, Moriyama S, Kanai Y, Nagamori S. 2022. Simple
1009 But Efficacious Enrichment of Integral Membrane Proteins and Their Interactions for
1010 In-Depth Membrane Proteomics. *Molecular & Cellular Proteomics* **21**:100206.
1011 doi:10.1016/j.mcpro.2022.100206
1012 Kragh-Hansen U, Sheikh MI. 1984. Serine uptake by luminal and basolateral membrane
1013 vesicles from rabbit kidney. *The Journal of Physiology* **354**:55–67.
1014 doi:10.1113/jphysiol.1984.sp015361
1015 Lee Y, Wiriyasermkul P, Jin C, Quan L, Ohgaki R, Okuda S, Kusakizako T, Nishizawa T, Oda
1016 K, Ishitani R, Yokoyama T, Nakane T, Shirouzu M, Endou H, Nagamori S, Kanai Y,
1017 Nureki O. 2019. Cryo-EM structure of the human L-type amino acid transporter 1 in
1018 complex with glycoprotein CD98hc. *Nature Structural & Molecular Biology* **26**:510–
1019 517. doi:10.1038/s41594-019-0237-7
1020 Liu J, Tan Y, Cheng H, Zhang D, Feng W, Peng C. 2022. Functions of Gut Microbiota
1021 Metabolites, Current Status and Future Perspectives. *Aging and disease* **13**:1106.
1022 doi:10.14336/AD.2022.0104
1023 Marx D, Metzger J, Pejchinovski M, Gil RB, Frantzi M, Latosinska A, Belczacka I, Heinzmann
1024 SS, Husi H, Zoidakis J, Klingele M, Herget-Rosenthal S. 2018. Proteomics and

1025 Metabolomics for AKI Diagnosis. *Seminars in Nephrology* **38**:63–87.
1026 doi:10.1016/j.semnephrol.2017.09.007
1027 Matsuo H, Chiba T, Nagamori S, Nakayama A, Domoto H, Phetdee K, Wiriyasermkul P,
1028 Kikuchi Y, Oda T, Nishiyama J, Nakamura T, Morimoto Y, Kamakura K, Sakurai Y,
1029 Nonoyama S, Kanai Y, Shinomiya N. 2008. Mutations in Glucose Transporter 9 Gene
1030 SLC2A9 Cause Renal Hypouricemia. *The American Journal of Human Genetics*
1031 **83**:744–751. doi:10.1016/j.ajhg.2008.11.001
1032 Metzner L, Kottra G, Neubert K, Daniel H, Brandsch M. 2005. Serotonin, L-tryptophan, and
1033 tryptamine are effective inhibitors of the amino acid transport system PAT1. *FASEB j*
1034 **19**:1468–1473. doi:10.1096/fj.05-3683com
1035 Miyauchi S, Abbot EL, Zhuang L, Subramanian R, Ganapathy V, Thwaites DT. 2005. Isolation
1036 and function of the amino acid transporter PAT1 (slc36a1) from rabbit and
1037 discrimination between transport via PAT1 and system IMINO in renal brush-border
1038 membrane vesicles. *Molecular Membrane Biology* **22**:549–559.
1039 doi:10.1080/09687860500421779
1040 Miyoshi Y, Hamase K, Tojo Y, Mita M, Konno R, Zaitsu K. 2009. Determination of D-serine
1041 and D-alanine in the tissues and physiological fluids of mice with various D-amino-acid
1042 oxidase activities using two-dimensional high-performance liquid chromatography
1043 with fluorescence detection. *Journal of Chromatography B* **877**:2506–2512.
1044 doi:10.1016/j.jchromb.2009.06.028
1045 Morehead RP, Fishman WH, Artom C. 1945. Renal Injury in the Rat Following the
1046 Administration of Serine by Stomach Tube. *The American Journal of Pathology*
1047 **21**:803–815.

1048 Mothet J-P, Parent AT, Wolosker H, Brady RO, Linden DJ, Ferris CD, Rogawski MA, Snyder
1049 SH. 2000. D-Serine is an endogenous ligand for the glycine site of the *N*-methyl-D-
1050 aspartate receptor. *Proc Natl Acad Sci USA* **97**:4926–4931. doi:10.1073/pnas.97.9.4926
1051 Nagamori S, Wiriyasermkul P, Guarch ME, Okuyama H, Nakagomi S, Tadagaki K, Nishinaka
1052 Y, Bodoy S, Takafuji K, Okuda S, Kurokawa J, Ohgaki R, Nunes V, Palacín M, Kanai
1053 Y. 2016a. Novel cystine transporter in renal proximal tubule identified as a missing
1054 partner of cystinuria-related plasma membrane protein rBAT/SLC3A1. *Proceedings of*
1055 *the National Academy of Sciences USA* **113**:775–780. doi:10.1073/pnas.1519959113
1056 Nagamori S, Wiriyasermkul P, Okuda S, Kojima N, Hari Y, Kiyonaka S, Mori Y, Tominaga
1057 H, Ohgaki R, Kanai Y. 2016b. Structure–activity relations of leucine derivatives reveal
1058 critical moieties for cellular uptake and activation of mTORC1-mediated signaling.
1059 *Amino Acids* **48**:1045–1058. doi:10.1007/s00726-015-2158-z
1060 Nakade Y, Iwata Y, Furuichi K, Mita M, Hamase K, Konno R, Miyake T, Sakai N, Kitajima
1061 S, Toyama T, Shinozaki Y, Sagara A, Miyagawa T, Hara A, Shimizu M, Kamikawa Y,
1062 Sato K, Oshima M, Yoneda-Nakagawa S, Yamamura Y, Kaneko S, Miyamoto T,
1063 Katane M, Homma H, Morita H, Suda W, Hattori M, Wada T. 2018. Gut microbiota–
1064 derived D-serine protects against acute kidney injury. *JCI Insight* **3**:e97957.
1065 doi:10.1172/jci.insight.97957
1066 Nakanishi N, Fukui M, Tanaka M, Toda H, Imai S, Yamazaki M, Hasegawa G, Oda Y,
1067 Nakamura N. 2012. Low Urine pH Is a Predictor of Chronic Kidney Disease. *Kidney*
1068 *and Blood Pressure Research* **35**:77–81. doi:10.1159/000330487
1069 Okada A, Nangaku M, Jao T-M, Maekawa H, Ishimono Y, Kawakami T, Inagi R. 2017. D-
1070 serine, a novel uremic toxin, induces senescence in human renal tubular cells via GCN2
1071 activation. *Scientific Reports* **7**:11168. doi:10.1038/s41598-017-11049-8

1072 Okushima H, Iwata Y, Hesaka A, Sugimori E, Ikeda T, Nakane M, Mita M, Hayashi T, Isaka
1073 Y, Kimura T. 2021. Intra-body dynamics of D-serine reflects the origin of kidney
1074 diseases. *Clinical and Experimental Nephrology* **25**:893–901. doi:10.1007/s10157-
1075 021-02052-5
1076 Papouin T, Ladépêche L, Ruel J, Sacchi S, Labasque M, Hanini M, Groc L, Pollegioni L,
1077 Mothet J-P, Oliet SHR. 2012. Synaptic and Extrasynaptic NMDA Receptors Are Gated
1078 by Different Endogenous Coagonists. *Cell* **150**:633–646.
1079 doi:10.1016/j.cell.2012.06.029
1080 Paroder V, Spencer SR, Paroder M, Arango D, Schwartz S, Mariadason JM, Augenlicht LH,
1081 Eskandari S, Carrasco N. 2006. Na^+/monocarboxylate transport (SMCT) protein
1082 expression correlates with survival in colon cancer: Molecular characterization of
1083 SMCT. *Proceedings of the National Academy of Sciences USA* **103**:7270–7275.
1084 doi:10.1073/pnas.0602365103
1085 Perland E, Fredriksson R. 2017. Classification Systems of Secondary Active Transporters.
1086 *Trends in Pharmacological Sciences* **38**:305–315. doi:10.1016/j.tips.2016.11.008
1087 Ranjan R, Khazen G, Gambazzi L, Ramaswamy S, Hill SL, Schürmann F, Markram H. 2011.
1088 Channelpedia: An Integrative and Interactive Database for Ion Channels. *Frontiers in*
1089 *Neuroinformatics* **5**. doi:10.3389/fninf.2011.00036
1090 Rosenberg D, Artoul S, Segal AC, Kolodney G, Radzishevsky I, Dikopoltsev E, Foltyn VN,
1091 Inoue R, Mori H, Billard J-M, Wolosker H. 2013. Neuronal D-Serine and Glycine
1092 Release Via the Asc-1 Transporter Regulates NMDA Receptor-Dependent Synaptic
1093 Activity. *Journal of Neuroscience* **33**:3533–3544. doi:10.1523/JNEUROSCI.3836-
1094 12.2013
1095 Sakaguchi YM, Wiriyasermkul P, Matsubayashi M, Miyasaka M, Sakaguchi N, Sahara Y,
1096 Takasato M, Kinugawa K, Sugie K, Eriguchi M, Tsuruya K, Kuniyasu H, Nagamori S,

1097 Mori E. 2024. Identification of three distinct cell populations for urate excretion in
1098 human kidneys. *The Journal of Physiological Science* **74**:1. doi: 10.1186/s12576-023-
1099 00894-0
1100 Sagné C, Agulhon C, Ravassard P, Darmon M, Hamon M, El Mestikawy S, Gasnier B, Giros
1101 B. 2001. Identification and characterization of a lysosomal transporter for small neutral
1102 amino acids. *Proceedings of the National Academy of Sciences USA* **98**:7206–7211.
1103 doi:10.1073/pnas.121183498
1104 Sasabe J, Suzuki M, Miyoshi Y, Tojo Y, Okamura C, Ito S, Konno R, Mita M, Hamase K, Aiso
1105 S. 2014. Ischemic Acute Kidney Injury Perturbs Homeostasis of Serine Enantiomers in
1106 the Body Fluid in Mice: Early Detection of Renal Dysfunction Using the Ratio of Serine
1107 Enantiomers. *PLoS ONE* **9**:e86504. doi:10.1371/journal.pone.0086504
1108 Sasabe J, Suzuki M. 2018. Distinctive Roles of D-Amino Acids in the Homochiral World:
1109 Chirality of Amino Acids Modulates Mammalian Physiology and Pathology. *The Keio*
1110 *Journal of Medicine* **68**:1–16. doi:10.2302/kjm.2018-0001-IR
1111 Scalise M, Pochini L, Console L, Losso MA, Indiveri C. 2018. The Human SLC1A5 (ASCT2)
1112 Amino Acid Transporter: From Function to Structure and Role in Cell Biology.
1113 *Frontiers in Cell and Developmental Biology* **6**:96. doi:10.3389/fcell.2018.00096
1114 Schweikhard ES, Ziegler CM. 2012. Amino Acid Secondary Transporters: toward a common
1115 transport mechanism. *Current Topics in Membranes* Elsevier. **70**:1–28.
1116 doi:10.1016/B978-0-12-394316-3.00001-6
1117 Shenkin A. 2006. Micronutrients in health and disease. *Postgraduate Medical Journal* **82**:559–
1118 567. doi:10.1136/pgmj.2006.047670
1119 Shimomura A, Carone FA, Peterson DR. 1988. Contraluminal uptake of serine in the proximal
1120 nephron. *Biochimica et Biophysica Acta (BBA) - Biomembranes* **939**:52–56.
1121 doi:10.1016/0005-2736(88)90046-6

1122 Silbernagl S, Völker K, Dantzler WH. 1999. D-Serine is reabsorbed in rat renal pars recta.
1123 *American Journal of Physiology-Renal Physiology* **276**:F857–F863.
1124 doi:10.1152/ajprenal.1999.276.6.F857
1125 Singer D, Camargo SMR, Huggel K, Romeo E, Danilczyk U, Kuba K, Chesnov S, Caron MG,
1126 Penninger JM, Verrey F. 2009. Orphan Transporter SLC6A18 Is Renal Neutral Amino
1127 Acid Transporter B^0AT3. *Journal of Biological Chemistry* **284**:19953–19960.
1128 doi:10.1074/jbc.M109.011171
1129 Srinivas SR, Gopal E, Zhuang L, Itagaki S, Martin PM, Fei Y-J, Ganapathy V, Prasad PD.
1130 2005. Cloning and functional identification of slc5a12 as a sodium-coupled low-affinity
1131 transporter for monocarboxylates (SMCT2). *Biochemical Journal* **392**:655–664.
1132 doi:10.1042/BJ20050927
1133 Stuart T, Butler A, Hoffman P, Hafemeister C, Papalexi E, Mauck WM, Hao Y, Stoeckius M,
1134 Smibert P, Satija R. 2019. Comprehensive Integration of Single-Cell Data. *Cell*
1135 **177**:1888-1902.e21. doi:10.1016/j.cell.2019.05.031
1136 Suzuki M, Shimizu-Hirota R, Mita M, Hamase K, Sasabe J. 2022. Chiral resolution of plasma
1137 amino acids reveals enantiomer-selective associations with organ functions. *Amino*
1138 *Acids* **54**:421–432. doi:10.1007/s00726-022-03140-w
1139 The UniProt Consortium, Bateman A, Martin M-J, Orchard S, Magrane M, Agivetova R,
1140 Ahmad S, Alpi E, Bowler-Barnett EH, Britto R, Bursteinas B, Bye-A-Jee H, Coetzee
1141 R, Cukura A, Da Silva A, Denny P, Dogan T, Ebenezer T, Fan J, Castro LG, Garmiri
1142 P, Georghiou G, Gonzales L, Hatton-Ellis E, Hussein A, Ignatchenko A, Insana G,
1143 Ishtiaq R, Jokinen P, Joshi V, Jyothi D, Lock A, Lopez R, Luciani A, Luo J, Lussi Y,
1144 MacDougall A, Madeira F, Mahmoudy M, Menchi M, Mishra A, Moulang K,
1145 Nightingale A, Oliveira CS, Pundir S, Qi G, Raj S, Rice D, Lopez MR, Saidi R,
1146 Sampson J, Sawford T, Speretta E, Turner E, Tyagi N, Vasudev P, Volynkin V, Warner

1147 K, Watkins X, Zaru R, Zellner H, Bridge A, Poux S, Redaschi N, Aimo L, Argoud-Puy
1148 G, Auchincloss A, Axelsen K, Bansal P, Baratin D, Blatter M-C, Bolleman J, Boutet E,
1149 Breuza L, Casals-Casas C, de Castro E, Echioukh KC, Coudert E, Cuche B, Doche M,
1150 Dornevil D, Estreicher A, Famiglietti ML, Feuermann M, Gasteiger E, Gehant S,
1151 Gerritsen V, Gos A, Gruaz-Gumowski N, Hinz U, Hulo C, Hyka-Nouspikel N, Jungo
1152 F, Keller G, Kerhornou A, Lara V, Le Mercier P, Lieberherr D, Lombardot T, Martin
1153 X, Masson P, Morgat A, Neto TB, Paesano S, Pedruzzi I, Pilbout S, Pourcel L, Pozzato
1154 M, Pruess M, Rivoire C, Sigrist C, Sonesson K, Stutz A, Sundaram S, Tognolli M,
1155 Verbregue L, Wu CH, Arighi CN, Arminski L, Chen C, Chen Y, Garavelli JS, Huang
1156 H, Laiho K, McGarvey P, Natale DA, Ross K, Vinayaka CR, Wang Q, Wang Y, Yeh
1157 L-S, Zhang J, Ruch P, Teodoro D. 2021. UniProt: the universal protein knowledgebase
1158 in 2021. *Nucleic Acids Research* **49**:D480–D489. doi:10.1093/nar/gkaa1100
1159 Uetsuka S, Ogata G, Nagamori S, Isozumi N, Nin F, Yoshida T, Komune S, Kitahara T,
1160 Kikkawa Y, Inohara H, Kanai Y, Hibino H. 2015. Molecular architecture of the stria
1161 vascularis membrane transport system, which is essential for physiological functions of
1162 the mammalian cochlea. *European Journal of Neuroscience* **42**:1984–2002.
1163 doi:10.1111/ejn.12973
1164 Vanslambrouck JM, Bröer A, Thavyogarajah T, Holst J, Bailey CG, Bröer S, Rasko JEJ. 2010.
1165 Renal imino acid and glycine transport system ontogeny and involvement in
1166 developmental iminoglycinuria. *Biochemical Journal* **428**:397–407.
1167 doi:10.1042/BJ20091667
1168 Vernocchi P, Del Chierico F, Putignani L. 2016. Gut Microbiota Profiling: Metabolomics
1169 Based Approach to Unravel Compounds Affecting Human Health. *Frontiers in*
1170 *Microbiology* **7**:1144. doi:10.3389/fmicb.2016.01144

1171 Wei L, Tominaga H, Ohgaki R, Wiriyasermkul P, Hagiwara K, Okuda S, Kaira K, Kato Y,
1172 Oriuchi N, Nagamori S, Kanai Y. 2016. Transport of 3-fluoro-L-α-methyl-tyrosine
1173 (FAMT) by organic ion transporters explains renal background in [^{18}F]FAMT positron
1174 emission tomography. *Journal of Pharmacological Sciences* **130**:101–109.
1175 doi:10.1016/j.jphs.2016.01.001
1176 Wickham H. 2010. A Layered Grammar of Graphics. *Journal of Computational and Graphical*
1177 *Statistics* **19**:3–28. doi:10.1198/jcgs.2009.07098
1178 Wiriyasermkul P, Nagamori S, Tominaga H, Oriuchi N, Kaira K, Nakao H, Kitashoji T, Ohgaki
1179 R, Tanaka H, Endou H, Endo K, Sakurai H, Kanai Y. 2012. Transport of 3-Fluoro-L-α-
1180 Methyl-Tyrosine by Tumor-Upregulated L-Type Amino Acid Transporter 1: A Cause
1181 of the Tumor Uptake in PET. *Journal of Nuclear Medicine* **53**:1253–1261.
1182 doi:10.2967/jnumed.112.103069
1183 Wiriyasermkul P, Moriyama S, Nagamori S. 2020. Membrane transport proteins in
1184 melanosomes: Regulation of ions for pigmentation. *Biochimica et Biophysica Acta*
1185 *(BBA) - Biomembranes* **1862**:183318. doi:10.1016/j.bbamem.2020.183318
1186 Wolosker H, Sheth KN, Takahashi M, Mothet J-P, Brady RO, Ferris CD, Snyder SH. 1999.
1187 Purification of serine racemase: Biosynthesis of the neuromodulator D-serine.
1188 *Proceedings of the National Academy of Sciences USA* **96**:721–725.
1189 doi:10.1073/pnas.96.2.721
1190 Wolosker H. 2018. The Neurobiology of D-Serine Signaling. *Advances in Pharmacology*
1191 **82**:325–348. doi:10.1016/bs.apha.2017.08.010
1192

1193 **Figures and Tables**

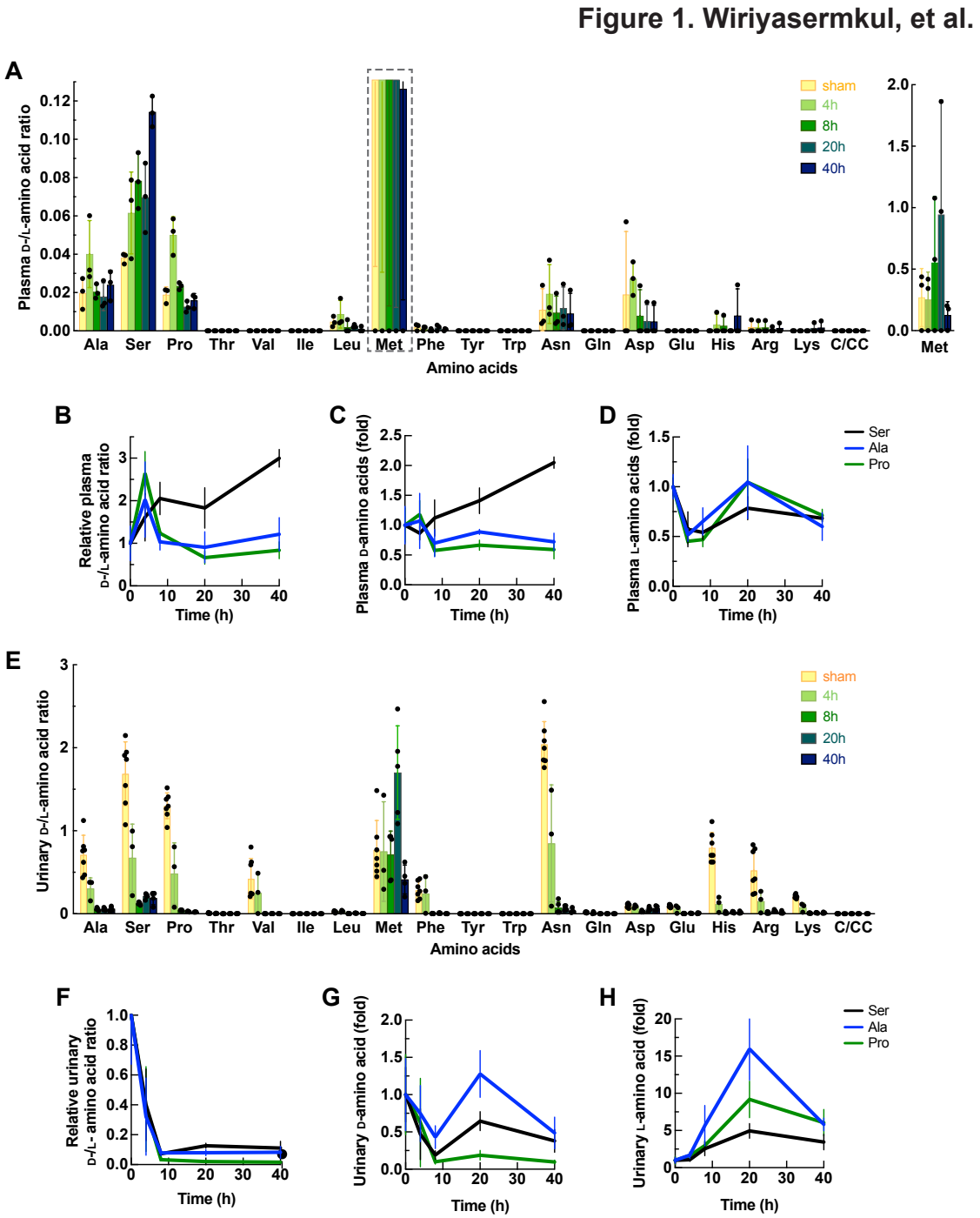

1194

1195 **Figure 1. Enantiomeric profiles of D- and L-amino acids in plasma and urine of the IRI**

1196 **model**

1197 Plasma and urine were collected from the mice after ischemia operation for 4, 8, 20, and 40 h
1198 or sham operation (0 h). The concentrations of twenty amino acids were measured by 2D-
1199 HPLC and plotted as mean ± SD. (**A**) Ratio of D-/L-amino acids from the plasma of the IRI
1200 model. The graph of Met is shown separately. n = 3. (**B**) – (**D**) Plasma amino acid profiles of
1201 serine, alanine, and proline from (**A**) were normalized with 0 h and plotted as ratios of D-/L-
1202 enantiomers (**B**), relative concentrations of D-isomers (**C**), and relative concentrations of L-
1203 isomers (**D**). (**E**) Ratio of D-/L-amino acids from the urine of the IRI model. n = 3 – 7. (**F**) –
1204 (**H**) Urinary amino acid profiles of serine, alanine, and proline from (**E**) were normalized with
1205 those at 0 h and plotted as ratios of D-/L- enantiomers (**F**), relative concentrations of D-isomers
1206 (**G**), and relative concentrations of L-isomers (**H**). C/CC: cysteine or cystine.

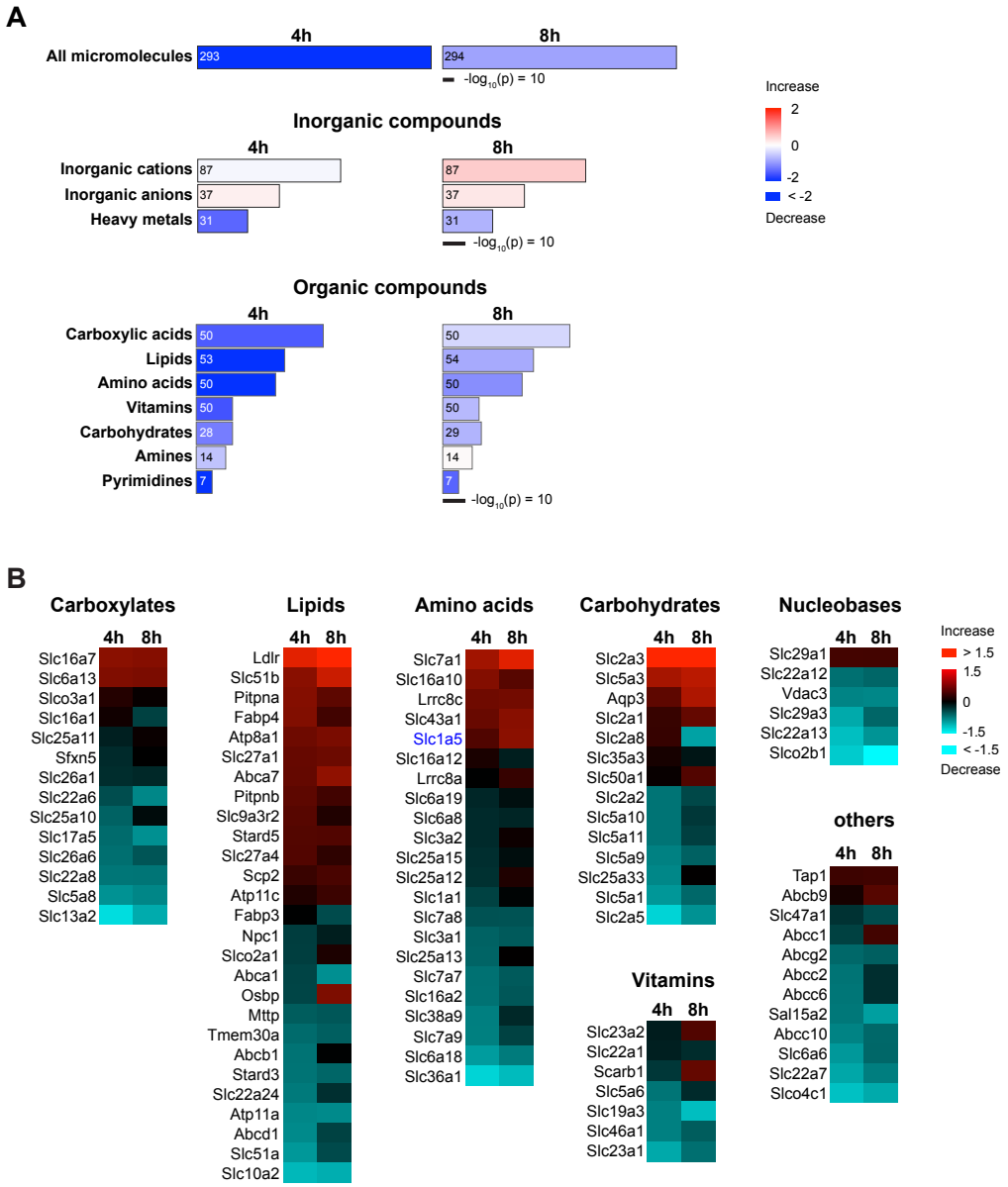

1207

1208 **Figure 2. *Molecular Transport* in renal BBMVs proteome of the IRI model**

1209 (**A**) Ingenuity Pathway Analysis (IPA) shows the heatmaps of *Molecular Transport* in the
1210 membrane proteome from BBMVs of the IRI model (4h IRI/sham (4h) or 8h IRI/sham (8h)).
1211 Transport functions are categorized by types of substrates. Transport of all micromolecules
1212 (top) is derived from the combination of inorganic (middle) and organic compounds (bottom).
1213 Area and colors represent -$\log_{10}$(p-value) and annotated functions (z-score), respectively.

1214 Numbers inside the columns indicate the numbers of corresponding proteins. (**B**) Heatmaps of
1215 membrane transport proteins that mediate the transport of organic compounds. The proteins
1216 with ratios of more than 1.1-fold change are shown. The category "others" includes the
1217 transport of peptides, organic cations, organic anions, and drugs. Colors indicate $\log_2$ fold of
1218 4h IRI/sham (4h) or 8h IRI/sham (8h).

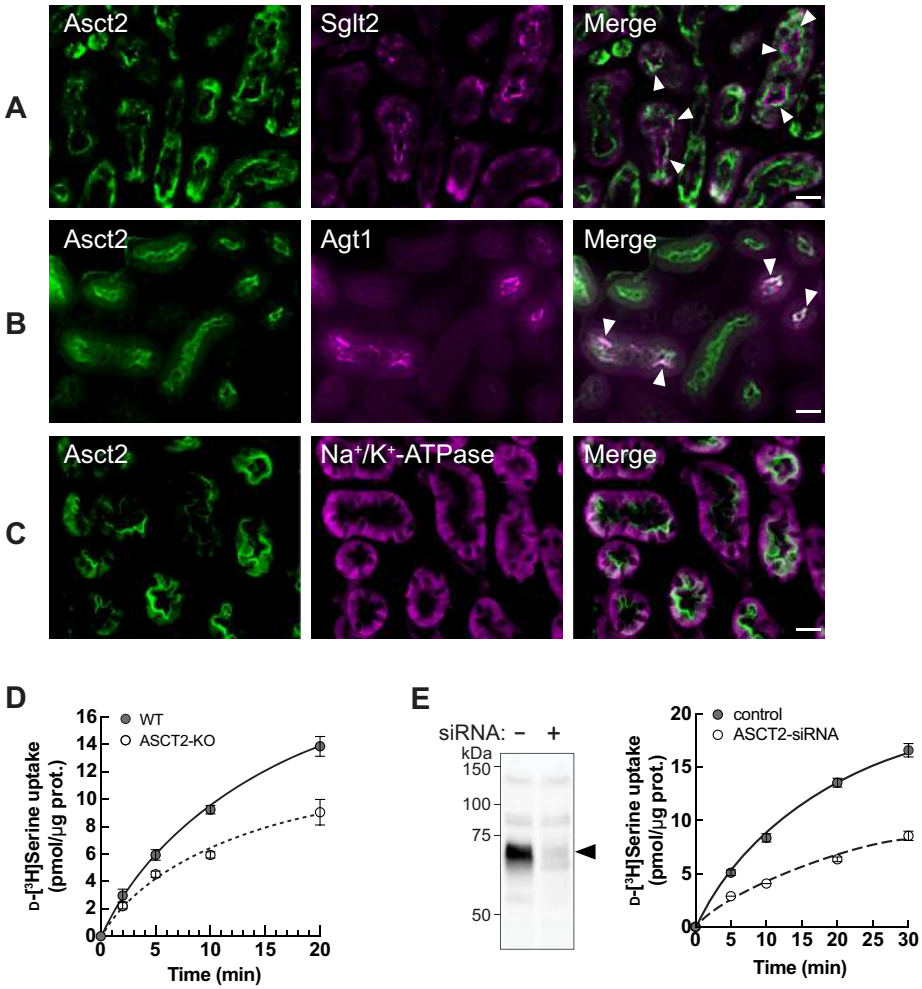

1219

1220 **Figure 3. ASCT2 is one of D-serine transporters at the apical membrane of renal proximal**
1221 **tubular epithelia.**

1222 (**A**) – (**C**) Localization of Asct2 in mouse kidney by immunofluorescence staining. Mouse
1223 kidney slides were co-stained with anti-Asct2(NT) antibody (Asct2; green) and protein markers
1224 for renal proximal tubule segments: anti-Sglt2 antibody (**A**: Sglt2, apical membrane marker of
1225 S1 + S2 segments), anti-Agt1 antibody (**B**: Agt1, apical membrane marker of S3 segment), and
1226 anti-Na^+/K^+-ATPase antibody (**C**: Na^+/K^+-ATPase, basolateral membrane marker). Merge
1227 images are shown in the right panel. Arrowheads indicate co-localization of the proteins. Scale
1228 bar = 20 μm. (**D**) Time course of 100 μM D-[^{3}H]serine transport in wild-type (WT) and *ASCT2*-

1229 knockout (ASCT2-KO) HAP1 cells measured in PBS pH 7.4. Dot plot = mean ± SEM; n = 3.

1230 **E**) Left: Western blot using anti-ASCT2 antibody verified the suppression of ASCT2 in

1231 ASCT2-siRNA transfected HEK293 cells. Right: Transport of 100 μM D-[^{3}H]serine (in PBS

1232 pH 7.4) was measured in ASCT2-knockdown (ASCT2-siRNA) in comparison to the Mock

1233 cells (control). Dot plot = mean ± SEM; n = 3.

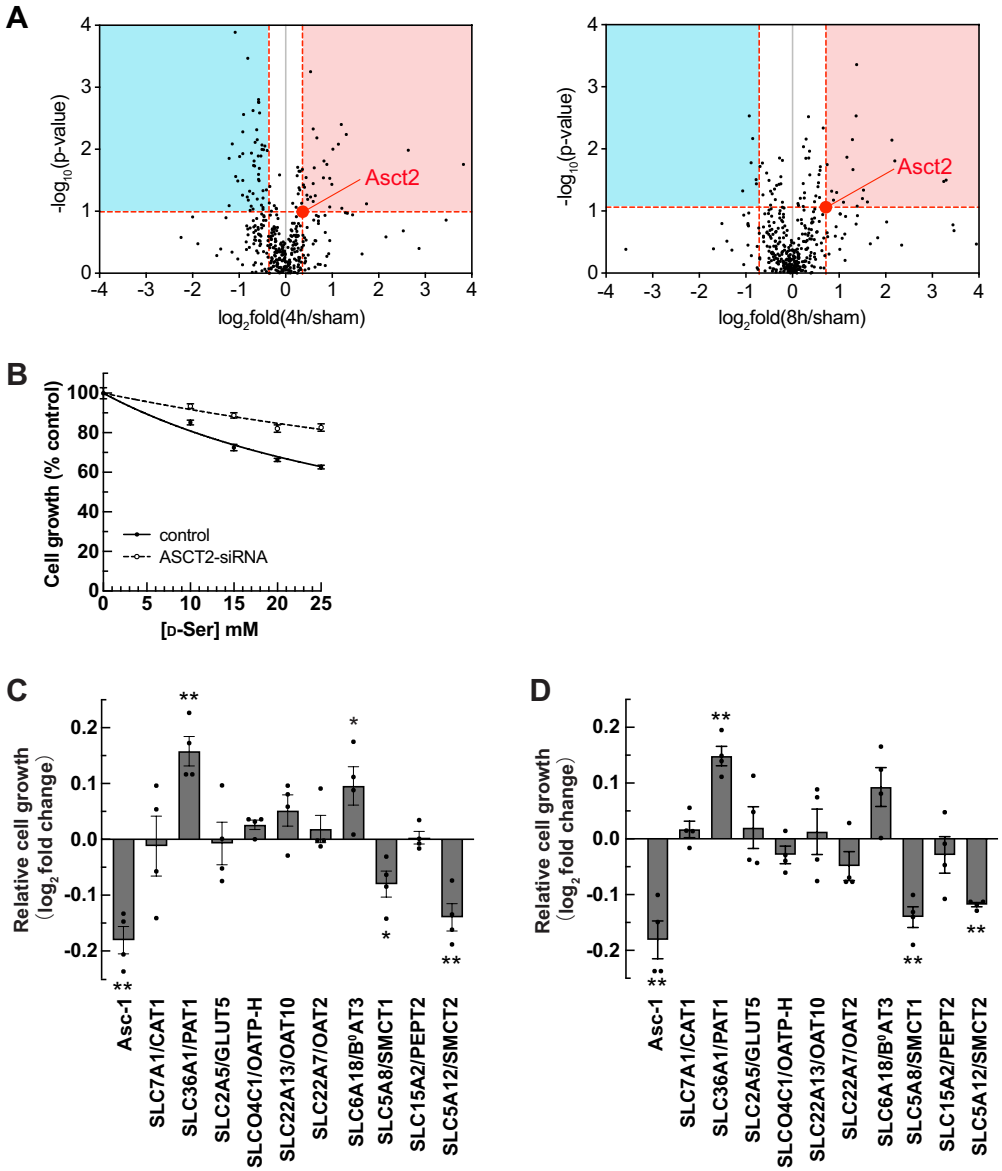

Figure 4. Identification of SMCT1 and SMCT2 as candidates of D-serine transporters

(**A**) Volcano plots of 398 membrane transport proteins identified from the BBMV proteome of the IRI model. The Median of $\log_2$ fold of 4h IRI/sham (left) or 8h IRI/sham (right) were plotted against $-\log_{10}$ of p-value. Three proteins with $\log_2$ fold more than 4.0 (see values in Table S1) are omitted for the better view. The value of Asct2 (red dot) was set as a cut-off value to select D-serine transporter candidates (both increased (red area) and decreased (blue area)

1241 expressions). (**B**) Cell-growth measurement (XTT assay) of ASCT2-siRNA or without siRNA
1242 (control) transfected HEK293 cells treated with D-serine. Data represent percent cell growth
1243 compared to the non-treated cells. The graphs were fitted to inhibition kinetics (Dose-response
1244 – Inhibition). Dot plot = mean ± SEM; n = 5. (**C**) – (**D**) Candidates of D-serine transporters
1245 were screened by cell-growth measurement. HEK293 cells were transfected with various
1246 cDNA clones, as indicated. After transfection, the cells were treated with either 15 mM (**C**) or
1247 25 mM (**D**) D-serine for two days and cell growth was examined. The growth effect by D-serine
1248 treatment was normalized with that of no treatment and then calculated as $\log_2$ fold change of
1249 Mock at the same D-serine concentration. Asc-1 is used as the positive control. Bar graph =
1250 mean ± SEM; n = 4; *$p < 0.05$; **$p < 0.01$.

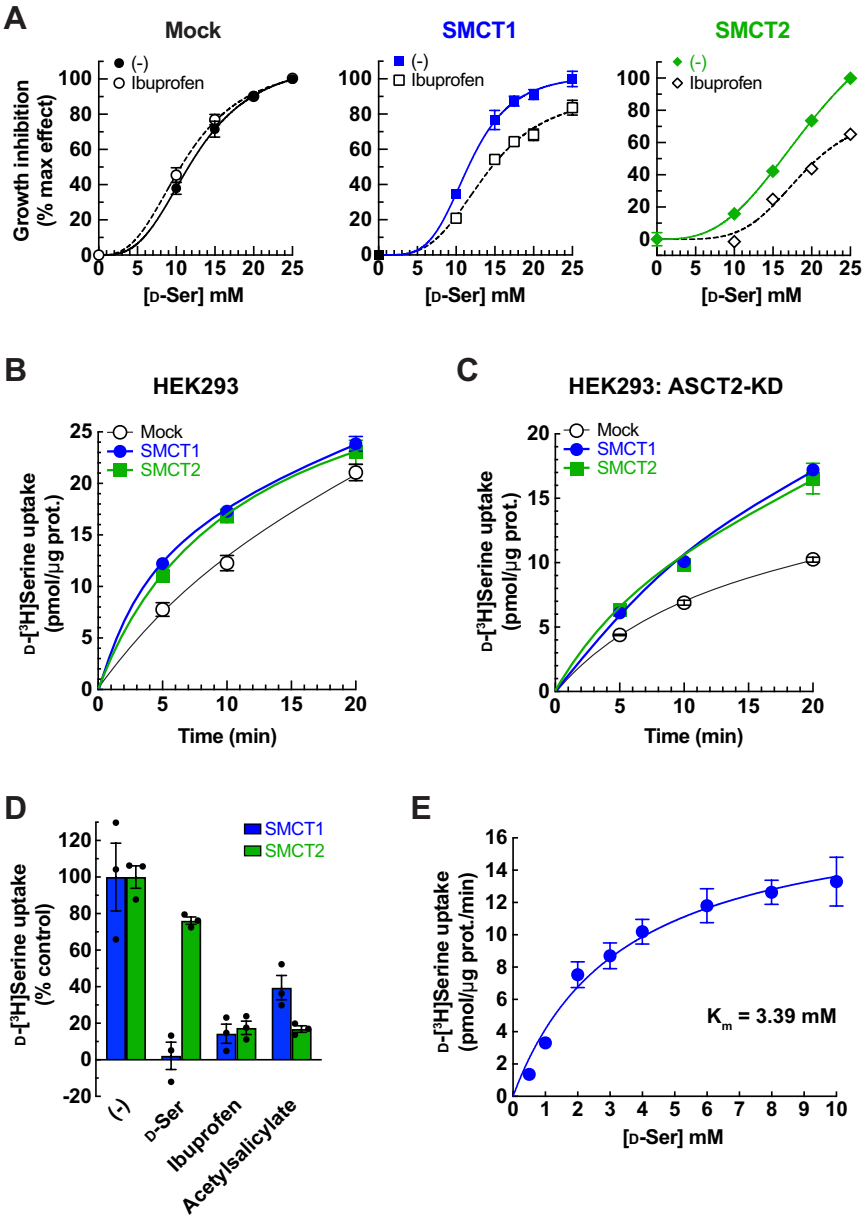

1251

1252 **Figure 5. Characterization of SMCT1 and SMCT2 as D-serine transporters using**
1253 **SMCT1- and SMCT2-stably expressing cells**

1254 (**A**) Inhibition effect of ibuprofen on D-serine-induced cell growth. FlpInTR-Mock (Mock),
1255 FlpInTR-SMCT1 (SMCT1), or FlpInTR-SMCT2 (SMCT2) cells were treated with D-serine
1256 for two days in the presence or absence of 0.5 mM ibuprofen. Cell growth was measured by
1257 XTT assay. For comparison, the maximum growth inhibition by 25 mM D-serine treatment was

1258 set as 100 % inhibition, and no D-serine treatment was set as 0 % inhibition. The graphs were
1259 fitted to inhibition kinetics (Dose-response – Inhibition). Dot plot = mean ± SEM; n = 5. (**B**)
1260 Time course of 100 μM D-[^{3}H]serine uptake in FlpInTR-SMCT1 (SMCT1), FlpInTR-SMCT2
1261 (SMCT2) and Mock cells. D-[^{3}H]Serine transport was measured in PBS pH 7.4. Dot plot =
1262 mean ± SEM; n = 4. (**C**) Time course of 100 μM D-[^{3}H]serine uptake was measured similarly
1263 to B), but the cells were subjected to ASCT2 knockdown (siRNA transfection) two days before
1264 the assay. Dot plot = mean ± SEM; n = 4. (**D**) Transport of 20 μM D-[^{3}H]serine by ASCT2-
1265 siRNA-transfected FlpInTR-SMCT1 or FlpInTR-SMCT2 stable cell lines were measured in
1266 the absence (-) or presence of 5 mM indicated inhibitors. The uptake was measured for 10 min
1267 in PBS pH 7.4. Graphs represented the uptake data subtracted from those of Mock cells. Bar
1268 graph = mean ± SEM; n = 3. (**E**) Concentration dependence of D-[^{3}H]serine transport in
1269 ASCT2-siRNA-transfected FlpInTR-SMCT1 cells. Uptake of D-[^{3}H]serine (0.5 – 10 mM) was
1270 measured for 10 min in PBS pH 7.4. Raw data was shown in Figure supplement 5D. The uptake
1271 data in FlpInTR-SMCT1 were subtracted from those of Mock cells and fitted to Michaelis-
1272 Menten plot with the apparent K_m of 3.39 ± 0.79 mM and V_{max} of 18.23 ± 1.73 pmol/μg
1273 protein/min. Dot plot = mean ± SEM; n = 3 – 4.

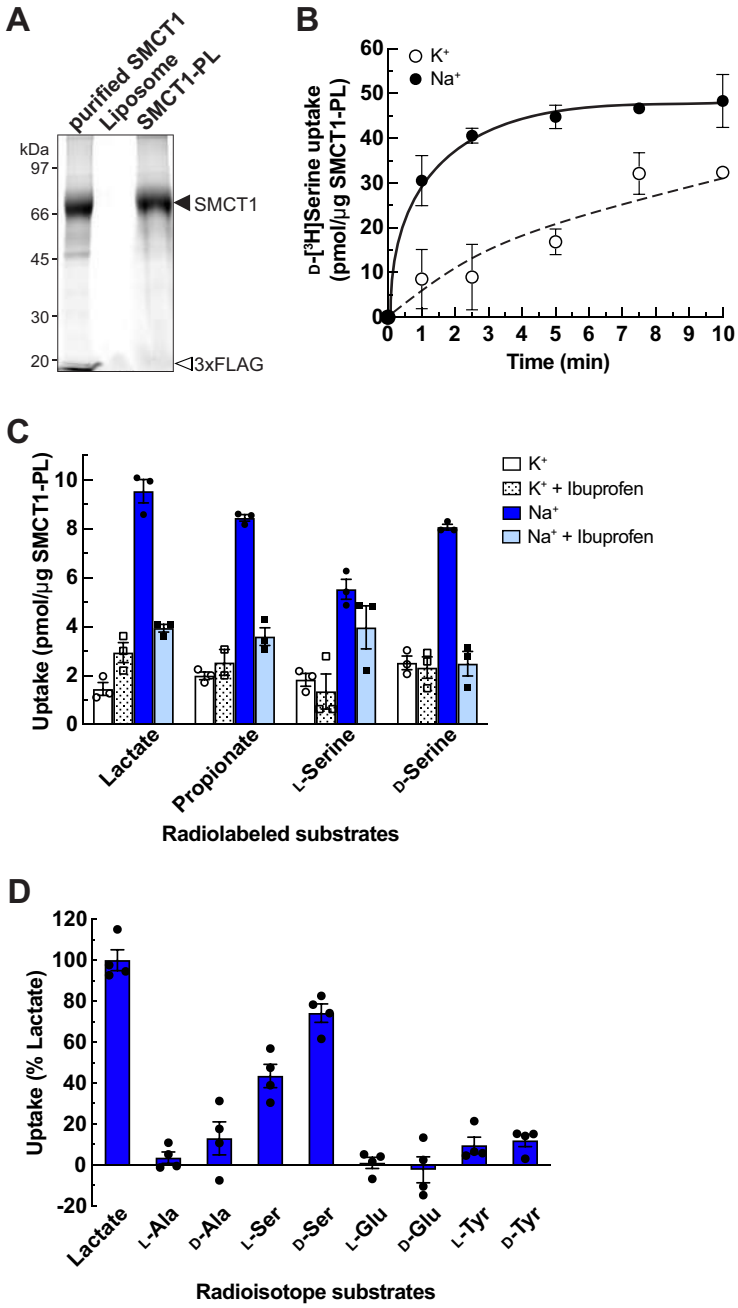

1274

1275 **Figure 6. Characterization of SMCT1 as D-serine transporter using SMCT1-**
1276 **reconstituted proteoliposomes (SMCT1-PL)**

1277 (**A**) Left: Stain-free SDS-PAGE gel shows SMCT1 (purified SMCT1) purified from pCMV14-
1278 SMCT1-transfected Expi293F cells, reconstituted empty liposomes (Liposome) and SMCT1-
1279 reconstituted proteoliposomes (SMCT1-PL). (**B**) Time course of D-[^{3}H]serine transport in

1280 SMCT1-PL. Uptake of 200 μM D-[^{3}H]serine was measured in Na^+-containing buffer (Na^+)
1281 compared to Na^+-free buffer (K^+). Dot plot = mean ± SEM; n = 3. (**C**) Ibuprofen effect on the
1282 uptake of [^{3}H]lactate, [^{3}H]propionate, L-[^{3}H]serine, and D-[^{3}H]serine in SMCT1-PL. Uptakes
1283 of 50 μM radiolabeled substrates were measured for 5 min in Na^+-containing buffer (Na^+) or
1284 Na^+-free buffer (K^+) in the presence or absence of 1 mM ibuprofen. Bar graph = mean ± SEM;
1285 n = 3. (**D**) Amino acid selectivity of SMCT1-PL. Transport of 50 μM radiolabeled amino acids
1286 was measured in SMCT1-PL for 5 min. The substrate uptake in Na^+-containing buffer was
1287 subtracted from those in Na^+-free buffer and calculated as % lactate uptake. Bar graph = mean
1288 ± SEM; n = 4.

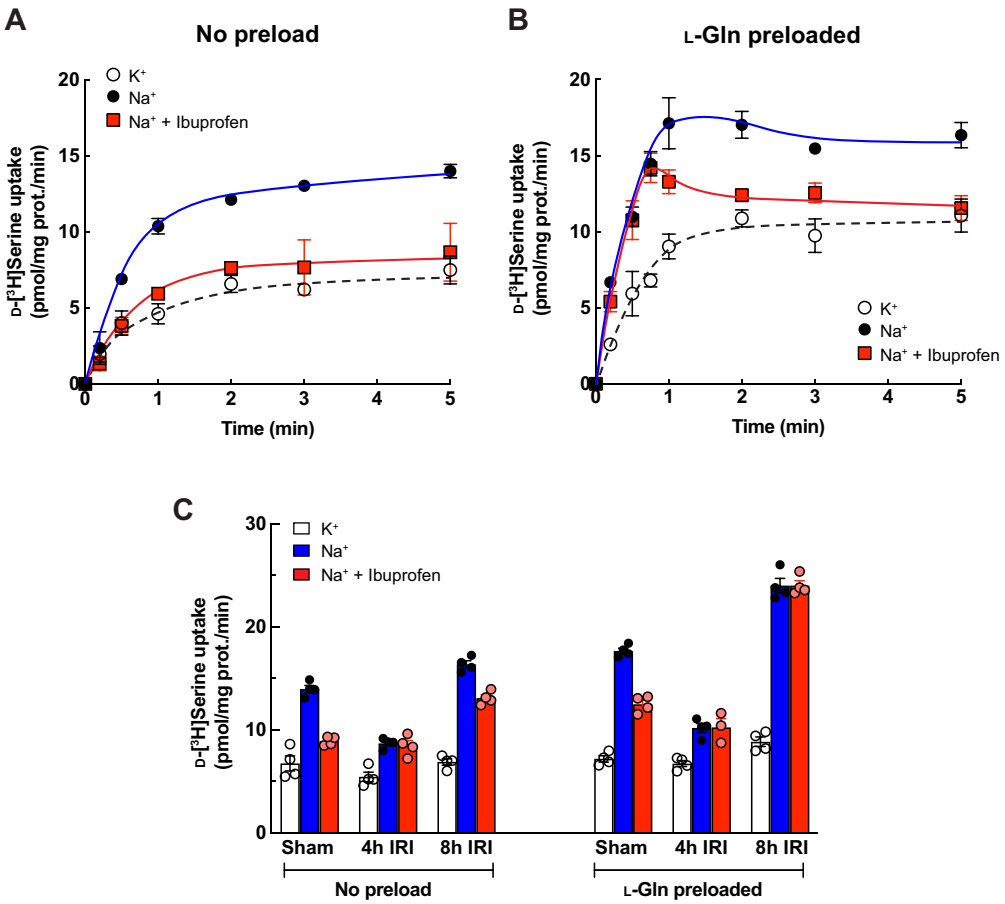

1289

1290 **Figure 7. Characterization of D-serine transporters in BBMVs of normal mice and the**

1291 **IRI model**

1292 (**A**) Transport of 10 μM D-[^{3}H]serine in renal BBMVs isolated from normal mice. The uptake

1293 was measured in Na^+-free buffer (K^+), Na^+-containing buffer (Na^+), or the presence of 1 mM

1294 ibuprofen (Na^+ + Ibuprofen). Dot plot = mean ± SEM; n = 3. (**B**) Transport of 10 μM D-

1295 [^{3}H]serine in renal BBMVs isolated from the normal mice was performed similarly to (**A**) but

1296 the BBMVs were preloaded with 4 mM L-Gln prior to the measurement. Dot plot = mean ±

1297 SEM; n = 4. (**C**). Transport of 10 μM D-[^{3}H]serine in renal BBMVs isolated from IRI model.

1298 Prior to uptake measurement, the BBMVs were preloaded with 4 mM L-Gln or buffer (no

1299 preload). The uptake was measured for 1 min in Na^+-free buffer (K^+), Na^+-containing buffer

1300 (Na^+), or the presence of 1 mM ibuprofen (Na^+ + Ibuprofen). Bar graph = mean ± SEM; n = 3

1301 – 4.

Figure 8. Wiriyasermkul, et al.

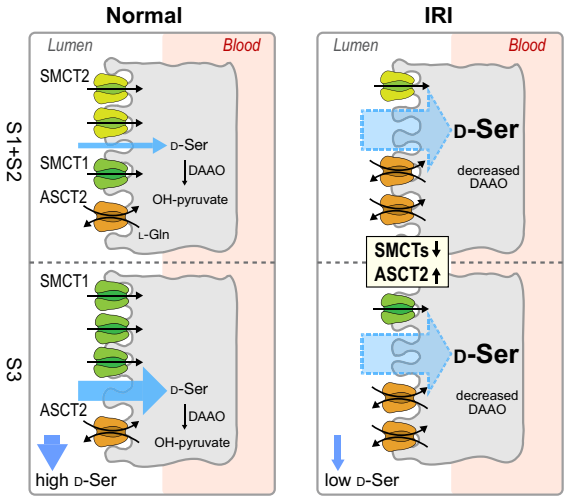

Figure 8. Proposed model of D-serine transport systems in renal proximal tubules

The model summarizes the contributions of ASCT2, SMCT1, and SMCT2 to D-serine transport in renal proximal tubules. Left: the physiological conditions (Normal kidney). SMCT2 at S1 + S2 segments and SMCT1 at segment S3 have high expression levels, whereas the expression of ASCT2 is low. The higher D-serine affinity of SMCT1 compared to SMCT2 supports that the D-serine reabsorption tends to be exceeded at the S3 segment. Right: the pathological conditions (IRI model). expressions of SMCTs decrease while that of ASCT2 increases. ASCT2 expresses ubiquitously and exhibits high D-serine affinity. Blue arrows anticipate total D-serine fluxes in each proximal tubular segment.

1313 **Table 1**. Candidate transporters from proteomics of the BBMVs from the IRI model. The list
1314 is ordered according to the fold change.

Transporters	Accession	log_2 fold 4h IRI/ sham	p-value of 4h IRI/ sham	log_2 fold 8h IRI/ sham	p-value of 8h IRI/ sham	Peptides	Score Mascot	Abundance in sham[a]
				Increased				
Slc7a1/Cat1	Q09143	0.8	0.12	1.3	0.01	1	131	2.6E+06
Slc1a5/Asct2	P51912	0.4	0.10	0.7	0.09	4	767	1.5E+07
				Decreased				
Slc36a1/Pat1	Q8K4D3	-1.2	0.08	-1.0	0.12	3	103	5.4E+06
Slc2a5/Glut5	Q9WV38	-1.2	0.01	-0.8	0.04	2	1,140	6.5E+07
Slco4c1/Oatp-m1	Q8BGD4	-1.1	0.00	-0.9	0.00	9	4,011	1.5E+08
Slc22a13/Oat10	Q6A4L0	-1.1	0.03	-0.8	0.03	15	5,948	5.6E+08
Slc22a7/Oat2	Q91WU2	-0.9	0.00	-0.6	0.02	13	6,100	4.3E+08
Slc6a18/B^0at3	O88576	-0.8	0.17	-0.6	0.25	11	4,310	2.1E+08
Slc5a8/Smct1	Q8BYF6	-0.8	0.05	-0.7	0.02	25	26,044	2.9E+09
Slc15a2/Pept2	Q9ES07	-0.7	0.01	-1.1	0.05	9	2,379	4.6E+07
Slc5a12/Smct2	Q49B93	-0.6	0.01	-0.9	0.01	12	4,725	1.6E+08
TMEM27/ Collectrin[b]	Q9ESG4	-0.4	0.01	-0.1	0.17	9	23,686	3.3E+09

[a]Median from n = 3
[b]Collectrin is a regulatory protein for B^0at3 function

1315